Spectral merging of MODIS / MERIS Ocean Colour Data to improve monitoring of coastal water processes

Fernanda Henderikx Freitas

March, 2009

Course Title:	Geo-Information Science and Earth Observation for Environmental Modelling and Management
Level:	Master of Science (Msc)
Course Duration:	September 2007 - March 2009
Consortium partners:	University of Southampton (UK) Lund University (Sweden) University of Warsaw (Poland) International Institute for Geo-Information Science and Earth Observation (ITC) (The Netherlands)
GEM thesis number:	2007-15

Spectral merging of MODIS / MERIS Ocean Colour Data to improve monitoring of coastal water processes

by

Fernanda Henderikx Freitas

Thesis submitted to the International Institute for Geo-information Science and Earth Observation in partial fulfilment of the requirements for the degree of Master of Science in Geo-information Science and Earth Observation for Environmental Modelling and Management

Thesis Assessment Board

Research Team Leader (Chair): Prof. Dr. Ing. Wouter Verhoef, (ITC)
External Examiner: Prof. Terry P. Dawson, University of Southampton (UK)
Internal Examiner: Dr. Yousif A. Hussin (ITC)
First Supervisor: Dr. Ir. Mhd. Suhyb Salama (ITC)
Second Supervisor: Dr. Ir. Chris M. Mannaerts (ITC)

ITC International Institute for Geo-Information Science and Earth Observation
Enschede, The Netherlands

Abstract

MODIS and MERIS are considered potential sensors for observing coastal oceanographic processes due to their appropriate spectral and spatial resolutions. In order to make use of the full spectral range provided by both sensors, a spectral merging technique was proposed. The method was tested for fifteen sampling points in the Santa Barbara Channel (SBC), California, for which field data was available (absorption coefficients and water-leaving reflectances). Because merging at any level requires that the data involved be as comparable and as free of errors as possible, Level 1B data from both sensors were pre-processed and atmospherically corrected utilising the same assumptions and algorithms. Since absorption and backscattering coefficients for the sampling units were either provided or calculated, a bio-optical model in the forward mode was used to estimate remote sensing reflectance for the complete range of wavelengths covered by MODIS and MERIS. Once all discrete wavelengths of one sensor had a common pair in the other sensor, a wavelength-based multi-linear regression was performed, having each sensor as an independent variable, and the field data (also modelled for the same wavelengths) as the dependent variable. The regression coefficients generated were tested for seven validation points. The merged spectra resulted in more accurate estimations of the field observations, if compared to the accuracy of the sensor's estimations alone. That was considered a positive result, as only a limited number of validation points were available, and the SBC region itself is highly variable in time and space. The bio-optical model was able to predict the original data at reference wavelength around 443 nm (<1% error), and the results obtained are highly dependent on the model's limitations and assumptions. In order to know if in practice the merged spectra can contribute with depicting information that the sensors alone cannot recognise, the technique should be applied for the whole region, rather than pixel-based, so that the processes could be directly observed. Important to notice that this work represents a first attempt in dealing with the complexity of merging radiometric units of sensors that are not commonly studied together because of their inherent differences. Despite the many limitations observed, it is believed that applying the technique for a larger number of sampling units or in a less complex environment could greatly improve the results obtained.

Acknowledgements

I still remember the amazing feeling of receiving the confirmation letter saying that I had gotten a scholarship to do a Masters in Europe! It was just so overwhelming, going away for 18 months, to a place I had always dreamed of going! And to leave family, friends, home and country behind…and to finish the undergrad thesis sooner than anyone else, running against the clock!

But it was so worth it! Thank you Mauricio, for forwarding that email to me…you've always believed in me, I am so grateful for that!

Thank you Lizi, Gaby, Chay, Ju, for the immeasurable support during those 2 months (and always!) Adoro vocês! Muitas saudades!

And how blessed I am to have gotten one more family! GEM, we've shared so much during those 18 months (literally!), I am really glad to have fallen inside this group…we are awesome! Hope to see everyone again very soon…Jose, Aidin, Mehdi, Betty, Prangya, Bhawna, Suz, Marcela, Maedeh…you guys are amazing! Daph, Kath, Rory, thank you so much for the loooong hours chatting, drinking tea, watching movies, making travel plans, getting lost somewhere, or doing nothing! I'll miss you so much!

To my supervisor, thank you for the opportunity. You introduced me to this whole new area of interest that I was clueless about, and that grew on me every single day. It's great to realise that despite all the challenges, I love what I do!

Mom, dad…what can I say?! You are everything to me, I'm so lucky to have you in my life…love you heaps!

To the E.U. and the Erasmus Mundus Programme, thank you for the opportunity and for the scholarship! I feel so lucky to have been part of all of this…that is one of those experiences you just never forget!

To Andre and the administrative staff, thanks for the support and understanding! It can't be easy to take care of all of us and of our complaints, so we really appreciated all you've done!

To the Santa Barbara University, NASA and ESA people, thank you for making data freely available, it's been a pleasure collaborating with the research on our oceans.

To all the other amazing people I've met during these 18 months…thanks for all the laughter, advices, cleaning parties, real parties, dinners and positive energy! Southampton, Lund, Warsaw, Enschede…I loved every bit of it!

Thank you God, and thank you Dudu, for watching us from wherever it is that you are…

And last but not least, thank you blooms, plumes, waves, greens and blues that make the coastal ocean such a fascinating subject to study! I'll never get over it!

Table of contents

List of figures

List of tables

1. Introduction

1.1. Observing the oceans through remote sensing: potentialities and limitations

Coastal waters are dominated by complex hydrographical processes, varying in time, space, and duration. To cite a few, currents vary in direction and speed according to hydro-dynamical conditions; rivers transport organic materials into the ocean, which are carried away by coastal currents; and seasonally, persistent wind blowing over a certain area, together with coastline orientation, provide conditions for upwelling episodes, determining areas where primary productivity is enhanced (Lalli and Parsons, 1997; Heap et al., 2001; Turner and Millward, 2002; Webster et al., 2003).

As part of specific Earth Observation missions (EO), remote sensing instruments such as MODIS, MERIS, SeaWiFS and POLDER have been collecting information on colour, chlorophyll concentration and temperature in the upper layer of the oceans for over 10 years. Every Earth Observation mission currently in space, however, presents limited global ocean coverage (Gregg et al., 1998). More interestingly, they capture information in different spectral, radiometric and spatial resolutions. Combining or **merging** different sources of information into a unique dataset has seemed like a logical alternative to not only increase data availability for a certain area, but to also increase the quality and type of information retrieved from the ocean.

There are many merging techniques currently being developed, and several of them under the NASA SIMBIOS program (McClain et al., 2002). The majority of the methods focus on merging final data products such as chlorophyll *a* and temperature (Gregg et al., 1998; Fargion et al., 2003; Pottier et al., 2006), although primary geophysical variables such as normalised water-leaving radiance and reflectance have also been used (Maritorena and Siegel, 2005;Mélin et al., 2008). Information on the different approaches can be found in IOCCG (2007).

Combining the datasets, however, is not a straight forward process. Different sensors have different specifications, orbits, spatial and spectral resolution; and, if the merging is based on already processed data, the difference between the algorithms, atmospheric corrections, and assumptions used are likely to result in uncertainty in the merged product. The practical motivation for using merging in ocean-colour studies is that statistically, provided the sensors used contribute with reliable data, a reduction in both stochastic and deterministic errors by increasing the number of measurements and by sensor inter-comparison and cross-validation should be expected (Mélin et al., 2008).

This M.Sc. aims to use a similar approach as of Maritorena and Siegel (2005) and Mélin et al (2008), who used a bio-optical model to merge MODIS and SeaWiFS normalised water-leaving radiance spectra for global and basin-scale applications. The present study aims to perform the same kind of spectral merging, but utilising MODIS and MERIS remote sensing reflectance data, in a local application: complex waters of the Santa Barbara Channel (SBC), Southern California, USA.

The main concerns regarding spectral merging are that the sensors do not capture information on the same discrete wavelengths, and that data must be cautiously calibrated and atmospherically corrected using the same algorithms and assumptions, in order to eliminate any source of errors that are not sensor-specific, and out of the scope of the researcher (Maritorena and Siegel, 2005; IOCCG, 2007; Morel et al., 2007).

Ultimately, merging data from sensors that measure a same region in different wavelengths may potentially result in retrieving more information from ocean colour than chlorophyll *a*, such as phytoplankton cell size, and backscattering by smaller particles, amongst others (Ciotti and Bricaud, 2006).

1.2. Why merging MODIS and MERIS data?

With the objective of learning about the individual performances of ocean colour sensors like SeaWiFS, MODIS and MERIS, many studies have been carried out in the last few years (Blondeau-Patissier, 2004; Bailey and Werdell, 2006; Zhang et al., 2006; Antoine et al., 2008; Bailey et al., 2008). In fact, projects with joint efforts of multiple organizations aimed to create “scientific quality ocean colour data sets encompassing measurements from multiple satellite missions” (Kwiatkowska and Fargion, 2002). As examples, SIMBIOS - Sensor Intercomparison for Marine Biological and Interdisciplinary Ocean Studies (Mueller et al., 1998), BOUSSOLE -

Bouée pour L'acquisition d'une Série Optique à Long Terme (Antoine et al., 2006) and GlobColour - European Node for Global Ocean Colour (ESA, 2005). The majority of the studies involving merging, however, have incorporated data from MODIS and SeaWiFS only (Maritorena and Siegel, 2005; Mélin et al., 2007), probably because those were developed within the same agency (NASA). When MERIS is included, the merging usually focus on Level 2 products like chlorophyll, and the type of water considered is normally Case-I (Fournier-Sicre and Belanger, 2002; Hu et al., 2007). In general, the conclusions have shown that SeaWiFS and MODIS products are better correlated to each other than any combination of those with MERIS products. However, studies utilising MERIS products for merging have only initiated recently. Hu et al (2007) and Antoine et al (2008) pointed out the need for MERIS data to be vicariously calibrated, as it could improve the quality of the retrieved data to some extent. According to the same authors, differences in the atmospheric correction schemes applied to each sensor are characterised as the major contributors to any inconsistency derived from their comparison. MERIS and MODIS together have been used in merging for land applications, and the resulting product was reported to be of decreased uncertainty and improved spatial coverage (Samain et al., 2006).

Sensor requirements for ocean observations reinforce the reasons behind choosing MODIS and MERIS in this study. In order to distinguish oceanographic variabilities and features over open oceans, an average bandwidth of 10 nm is required for the bands located in the visible part of the spectrum (ESA, 2006). In order to resolve the spectral features of the oxygen absorption band occurring at 760 nm, which is important for calibration purposes, a minimum spectral bandwidth of 2.5 nm is required (ESA, 2006). Spectral information retrieved from the red-edge (~700 nm) has shown to provide accurate estimates of chlorophyll, and to date, MERIS is the only sensor capable of retrieving data over that spectral region (Dall'Olmo et al., 2005). The fact that MODIS and MERIS' register data in different parts of the spectrum, apart from one common wavelength, is also promising when one is focusing on spectral merging. And finally, over coastal waters, increased spatial resolution is advised in order to observe the small scale processes inherent of these waters, which is a reason for not including SeaWiFS data (4.9 km spatial resolution). Currently, MERIS and MODIS are believed to be successful candidates for analysing coastal and oceanic waters. Moreover, this study intends to cooperate with the current trend of standardising and comparing data provided by different agencies, while contributing with more material on MERIS instrument, and merging of two sensors for coastal water monitoring. MODIS and MERIS' basic specifications follow in Table 1.

Table 1 Sensor's specifications. Compiled from (ESA, 2006; GSFC/NASA, 2007; Bourg et al., 2008).

Specifications	MERIS		MODIS (Aqua)	
Name	Medium Resolution Imaging Spectrometer		Moderate Resolution Imaging Spectroradiometer	
Agency	European Space Agency (ESA)		National Aeronautics and Space Administration (NASA)	
Satellite	Envisat		Aqua	
Launched on	March 2002		May 2002	
Software	BEAM – Visat		SeaDAS	
Altitude	800 km		705 km	
Spatial Resolution	1040m x 1200m (reduced) or 260m x 300m (full)		1000m x 1000m for ocean bands	
Swath Width	1150 km		2330 km	
Viewing angle	68.5^o		+/- 55^o	
Imaging method	Push-broom		Whisk-broom	
Equator crossing time	10:30 (descending node)		13:30 (ascending node)	
Revisit time	~3 days		~2 days	
Repeat cycle of reference orbit	35 days		16 days	
Known corrections to be performed	Smile effect[1a]		Bowtie effect[1b]	
Default geolocation	Ellipsoid WGS84		Sinusoidal Projection	
Solar spectral range	Reflective		Reflective and emissive	
Number of pixels in Rows/columns	1121 / 1121 (reduced res.) 2241 / 2241 (full resolution)		1354 / 2030 (ocean bands)	
Wavebands	15, in the VIS and NIR		36: 20 in the VIS and NIR, 10 in the SWIR, and 6 in the LWIR	
Ocean colour bands	*Centre*	*Width (nm)*	*Centre*	*Width (nm)*
	412.5	10	412.5	15
	442.5	10	443	10
	490	10	488	10
	510	10	531	10
	560	10	551	10
	620	10		
	665	10	667 (hi/lo)	10
	681.25	7.5	678 (hi/lo)	10
	708.75	10		
	753.75	7.5	748	10
	761.875	3.75		
	778.75	15		
	865	20	869.5	15

[1a] Smile effect: Small-scaled variations of the central spectral wavelength of each pixel along the images caused by differences in calibration between the 5 CCD (*charge coupled device*) sensors equipped within MERIS. The "Smile" effect refers to the spectral dispersion law observed (Bourg et al., 2008).
[1b] Bowtie effect: A distortion effect (oversampling of pixels around the edges of the scene) due to the scanning mode of MODIS, which images 10 lines at a time, as opposed to other sensors like SeaWiFS, which scans only 1 at a time.

1.3. Interaction between light and water constituents

In the ocean, light propagates through the air-sea interface and interacts with its constituents in diverse directions and intensities (Tzortziou et al., 2006; Doxaran et al., 2007). Eventually, fractions of light leave the water surface and reach the satellite-borne sensors, carrying with it information about the water (Loisel and Stramski, 2000). Optically significant constituents of sea water include phytoplankton, suspended sediments, chromophoric dissolved organic matter (CDOM), marine snow, detritus and the water itself (Jerlov, 1976; Campbell, 1996; Perry, 2003; Twardowski et al., 2004). Each of them has a unique optical signature, defined by their Inherent Optical Properties (IOPs) of absorption, scattering, attenuation and fluorescence. IOPs modify the incoming solar radiation, determining the characteristics of the water field, which corresponds to the Apparent Optical Properties of the water (AOP), associated with the ocean's colour and clarity (Bissett et al., 2005). AOPs include upwelling radiance and downwelling irradiance. When treated as a ratio, those represent the remote sensing reflectance, a primary ocean colour variable (Mobley, 1994; Perry, 2003). IOPs (specially absorption and scattering) and AOPs (remote sensing reflectance) are related via Reflectance Models (Gordon et al., 1975; Mobley, 1994). For further information on the equations considered, refer to Chapter 3.

Spectral behaviour of water constituents

Photosynthetic organisms (phytoplankton) absorb electromagnetic radiation predominately in the blue, blue-green, and red portions of the visible spectrum, depending on pigment composition. Bricaud et al (1981) states that generally, the maximum absorption by algal pigment is around 440 nm. As particles, they scatter light, and the shape of the scattering spectrum is dependent on phytoplankton size (which is highly variable - from 0.7 μm to 100 μm), composition, and absorption spectrum. Fluorescence by phytoplankton and CDOM is observed around 680 nm

(Perry, 2003). Suspended sediments predominately scatter light, although iron-rich minerals in the water are strong absorbers (Babin and Stramski, 2002). The scattering spectrum of both organic particles and sediments depend on their size distribution (Perry, 2003). Identifying or separating amongst the different constituent's optical signatures is a challenging subject in Case-II waters, as even though they co-exist, they are not necessarily co-variant in these optically complex regions (Morel and Prieur, 1977; Magnuson et al., 2004; Dall'Olmo et al., 2005; Boss et al., 2007).

1.4. Research Approach

1.4.1. General Objective

To perform spectral merging of MODIS-Aqua and MERIS Ocean Colour data in order to improve the understanding of coastal water processes in the Santa Barbara Channel, California.

1.4.2. Specific Objectives

1) To perform a spectral-based merging technique between MODIS-Aqua and MERIS remote sensing reflectance data in the Santa Barbara Channel area;
2) To investigate if improvement in accuracies are achieved with the merged products, regarding estimating the values obtained in the field;
3) To investigate if merged data results in better representation of the oceanographic conditions in the study area, in terms of depicting spectral features that the sensors alone are not able to depict.

1.4.3. Research Questions

1) Despite MODIS and MERIS' inherent differences in spectral and spatial resolution, design and orbit patterns, is it possible to perform a spectral merging of their remote sensing reflectance estimations in the SBC?
2) Does merging MODIS and MERIS remote sensing reflectances improve the accuracy of the final retrievals (in terms of how similar those results are from reflectances collected in the field)?
3) Considering that more discrete wavelengths will determine the merged spectrum, will more oceanographic features actually be depicted?

1.4.4. Research Hypotheses (H_0)

1) -
2) Merging MODIS and MERIS remote sensing reflectance data does not improve the accuracy of the field estimations;
3) Regardless of the increase in the number of discrete wavelengths available after merging MODIS and MERIS data, the same features and oceanographic structures will be depicted if compared to the observed by the sensors alone.

2. The Santa Barbara Channel Region

The Santa Barbara Channel (SBC) is located in Southern California, western USA. It is approximately 100 km long by 40 km wide, bordered on the south by four islands (whose land and surrounding waters are protected as The Channel Islands National Park and The Channel Islands Marine Sanctuary) and on the north by the coastal zone (Figure 1). It is a typical Case-II water environment, highly productive, with ocean colour varying according to phytoplankton blooms, sediment plumes, brown tides, oil spills, continental runoff, and mixing of diverse water masses (Toole and Siegel, 2001). Reflectances tend to be driven by absorption at 443 nm and by backscattering at 555 nm, characterising the water colour as green to bluish green (Toole and Siegel, 2001). Chlorophyll *a* concentrations usually reach 20 mg/m^3 in the channel, with a mean around 2 mg/m^3 (Kostadinov et al., 2007).

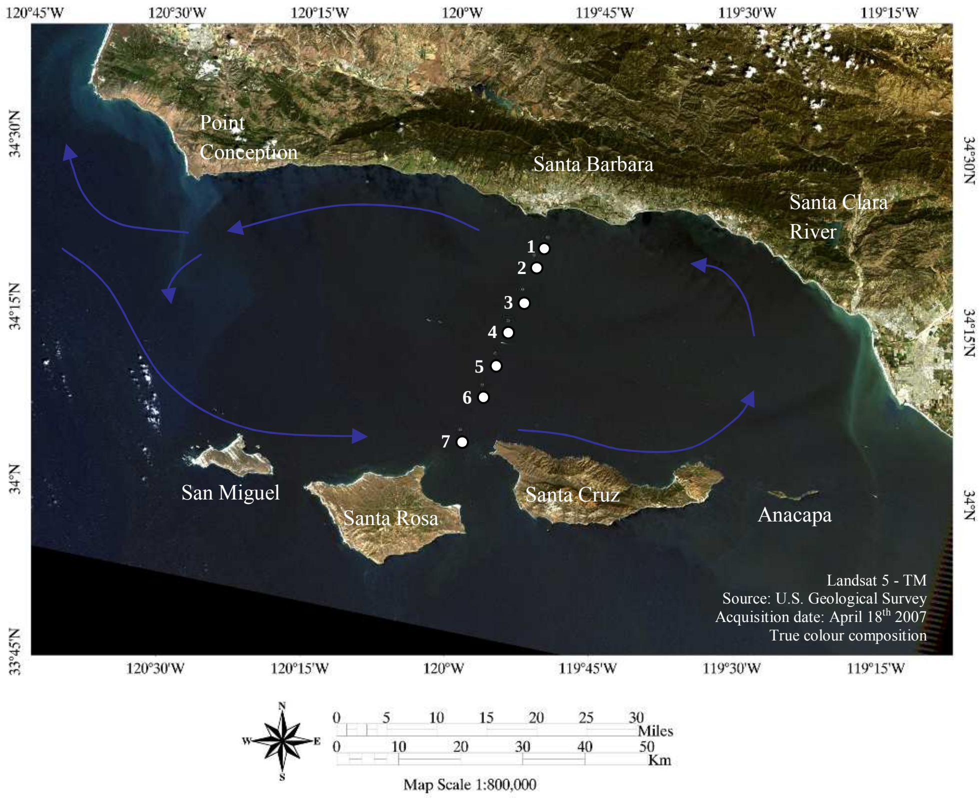

Figure 1 The Santa Barbara Channel and its vicinities. Crossing the channel are the seven sampling stations where the data used in this study was retrieved from, along with their numbers of reference. Distance between points is approximately 6 km, with the last point being relatively further from the others. The Landsat image captures two coastal processes highly variable in space and time: the runoff from Santa Clara River and the upwelling in Point Conception, triggered by the coastline orientation and wind regimes. The blue lines represent the usual water flow direction in the surface, controlled by the Californian Current (adapted from Harms and Winant, 1998). Vector lengths are not scaled to represent flow intensity. For a bathymetric map of the region, refer to Appendix I.

Currents in the channel are believed to mirror both a "larger-than-SBC" scale atmospheric flow, and a cyclonic circulation specific to the channel, causing surface currents to flow in divergent directions within the channel limits (Harms and Winant, 1998) (See Figure 1). Resulting from the divergent forces around the edges, flow velocities are very small in the middle section, which can trap water masses of certain temperature and phytoplankton blooms. The circulation system is controlled by the California Current, which is seasonally divided into an equatorward flow of fresh and cold water from the north Pacific, and its seasonal variations under the form of sub-surface or superficial poleward flows, that also re-circulate the warmer and more saline waters inshore (Bray et al., 1999). Surface water temperature ranges from 10 to 20^{o}C, with an average of 15^{o}C, as a result of the persistence of the cold California Current in the area (Otero and Siegel, 2004; Kostadinov et al., 2007).

The presence of different water masses throughout the year depend on river discharges from the west (Point Conception) or east of the region (Santa Clara River); on upwelling around Point Conception (which is also the major source of nutrients for the area); and on the propagation of cyclones of smaller magnitudes within the channel (Atkinson et al., 1986; Harms and Winant, 1998). Logically, those are related to the wind regime of the area: during fall and winter, storms dominate the wind conditions, resulting in terrestrial runoff and coastal resuspension; during spring and all through summer, persistent winds hit along the Californian coast and intensify upwelling episodes (Otero and Siegel, 2004). Intense flooding episodes in the watersheds have been linked to El Niño climatic conditions. The short time-lag between rainfall and runoff implies that sediment plumes in the coastal areas could potentially be observed a few hours after the storms (Mertes et al., 1998).

Climate in the region is characterised by mild and moist winters, and warm and dry summers (Mertes et al., 1998). Coastal fog controls air temperature variations, ranging from 10^{o}C in January to over 38^{o}C in the summer months (Mertes et al., 1998). Yearly precipitation is around 400 mm (State of California, 2007).

The Plumes and Blooms program, a joint collaboration among the University of California, Santa Barbara (UCSB) faculty, student and staff researchers at the Institute of Computational Earth System Science (ICESS), NOAA researchers at the Coastal Services Center (Charleston, SC), and the NOAA sanctuary managers of the Channel Islands National Marine Sanctuary (CINMS), has been collecting environmental and oceanographic data on the SBC since 1996 (ocean colour spectra, temperature, chlorophyll *a* concentration, etc). Such efforts reflect the economical and environmental importance of the area (which is composed of Marine Protected Areas, densely populated coastal cities and harbors) as far as monitoring the various coastal processes and management of natural resources.

Plumes and Blooms' ("PnB") field campaign sampling sites are shown in Figure 1. The data used in this M.Sc. corresponds to the same points, as they belong to the same program.

3. Methods

3.1. Data and Software

An overview of all the data and software compiled and used in this M.Sc. follows.

Images

- 5 L1B and L2 MODIS/MERIS images from the period 2003 – 2007, cloud-free around the Santa Barbara Channel, in Californian coastal waters (USA) (scenes centred on lat/long 34.2 N /-119.8 W). These images are match-ups with field campaign from the "Plumes and Blooms" experiment of the NOMAD project (NASA bio-Optical Marine Algorithm Dataset) (Werdell and Bailey, 2005). Wavelength range extracted: 412 – 870 nm, and sun zenith angles. Information on the images selected follow in Table 2.

Table 2 Images' IDs as they are ordered for MODIS L1B 1km spatial resolution and MERIS L1B Reduced Resolution (RR) of 1.2 km. In blue, the acquisition time (GMT) in the format HHMM for MODIS and HHMMSS for MERIS.

Date	MODIS ID (Level 1B)	MERIS ID (Level 1B)
15/01/2003	MYD021KM.A2003015.2125	MER_RR__1PQBCM20030115_180904
21/06/2005	MYD021KM.A2005172.2035	MER_RR__1PQBCM20050621_180124
21/03/2006	MYD021KM.A2006080.2120	MER_RR__1PQBCM20060321_182117
15/11/2006	MYD021KM.A2006319.2040	MER_RR__1POBCM20061115_180904
11/12/2007	MYD021KM.A2007345.2045	MER_RR__1PPBCM20071211_182205

MODIS images were acquired as part of the NASA's Earth-Sun System Division and archived and distributed by the Goddard Earth Sciences (GES) Data and Information Services Center (DISC) Distributed Active Archive Center (DAAC). For direct access: www.ladsweb.nascom.nasa.gov.

MERIS images can be ordered via the BEAM/VISAT software. For information on downloading the images, consult
http://www.brockmann-consult.de/beam/doc/help/general/BeamDataSources.html

Field measurements

- Remote-sensing reflectances for just below the water surface in 5 wavelengths (412, 443, 490, 510 and 555 nm) for 7 points between the Channel Islands and the Californian mainland, for the same dates of the images selected; spectra of absorption coefficients (a_{ph}, a_g and a_d) from 400 to 700 nm, in 2 nm increments and; total surface chlorophyll *a* data (in mg/m^3). The data is part of the Plumes and Blooms experiment, and was kindly provided by David Court, from the University of Santa Barbara (USA), after an email request. The same data was published by (Kostadinov et al., 2007). Some details follow in Table 3. For information on stations location, refer to Chapter 2.

Table 3 IDs, dates and sampling period of the field measurements. Measurements or water collection in each of the available stations were made within 3-4 minutes.

Cruise ID	Date	Sampling period per cruise (GMT)	Stations available, in the order they were visited
PnB-142	15/01/2003	17:00 – 22:00	7, 6, 5, 4, 3, 2, 1
PnB-174	21/06/2005	15:00 – 20:00	7, 6, 5, 4, 3, 2, 1
PnB-184	21/03/2006	16:30 – 19:00	7, 6, 5, 4
PnB-189	15/11/2006	17:30 – 22:00	7, 6, 5, 4, 3, 2, 1
PnB-199	11/12/2007	17:00 – 18:00	3, 2, 1

Other data

- Spectra of specific absorption coefficients b_w and a_w (Smith and Baker, 1978; Pope and Fry, 1997);
- Optimised absorption by phytoplankton spectra (a^*_{ph} (λ)) for the SBC area, from Kostadinov et al (2007).
- Extraterrestrial irradiance $[F_0\ (\lambda)]$ from Thuillier et al (2003);
- Daily Earth-Sun distances, from the Jet Propulsion Laboratory website (http://ssd.jpl.nasa.gov/horizons.cgi#top)
- Bathymetry contours of Santa Barbara Channel (Ocean Explorers, 2007);
- Precipitation records around the Santa Barbara Basin, from State of California - Department of Water Resources (2007).
- MODIS sea-surface temperature (SST) and chlorophyll-*a* data for the same dates of the L1B images, downloaded from http://oceancolor.gsfc.nasa.gov/cgi/browse.pl. (In Appendix IV).
- Essential publications providing model constants and formulas: Gordon et al (1988), Mobley (1994), Maritorena et al (2002), Kostadinov et al (2007).

Processing software

- ENVI v. 4.4 (from ITT Visual Information Solutions, at www.ittvis.com);
- BEAM-VISAT v. 4.2 (ENVISAT /ESA Brockmann Consult and contributors, freely available at http://www.brockmann-consult.de/beam/); – to get calibration coefficients for MERIS; to correct for the Smile Effect;

to project MERIS data; and to easily get illumination angles for both MODIS and MERIS (easy-to-use layer analysis), needed to perform atmospheric correction;

- STATISTICA v.6.0 for Multi-linear Regression analysis;
- Microsoft Excel 2003; - to perform bio-optical inversion and forward modelling of wavelengths.

Supporting software:

- HDFView – to read MODIS metadata;
- MATLAB v. 7.6.0 (R2008a) (From The MathWorks, Inc) - for data interpolation;
- GRAPHER v. 5.02 (Golden Software, Inc.) – for graphing presentation;
- ENDNOTE X1 0.1. (Thomson, available at www.endote.com) - for text referencing;
- ENVI plug-in for Ocean Colour (EPOC) - for re-projection of the MODIS L2 data (chl-a and SST), freely available at http://www.ittvis.com/Downloads/toolkits.aspx.

3.2. Structure: Flow-diagrams

In order to get into merging of MERIS and MODIS datasets, a summary of the methodology to be presented follows:

- Pre-processing: Radiometric standardization of MODIS and MERIS L1B data;
- Atmospheric correction of the images;
- Reflectance model in inverse and forward mode to estimate water-leaving reflectance in extra wavelengths, for both sensors and for field data;
- Wavelength-based multi-linear regression between MODIS and MERIS' spectrum signatures to retrieve coefficients of an equation that is assumed to better predict the field measurements;
- Validation of the results with independent data, and interpretation of the outputs.

Detailed flow-diagrams explaining the various parts are found in Appendix II, as they may serve as consultation along the reading.

3.3. In-situ measurements

Following information provided by David Court (communication via email, Dec. 2008) and Kostadinov et al (2007), profiles of upwelling radiance, $L_u(\lambda)$, and downwelling irradiance, $E_d(\lambda)$ at 5 wavelengths (412, 443, 490, 510 and 555) were obtained with a PRR-600 (*Biospherical Instruments Profiling Reflectance Radiometer,* by Biospherical Instruments Inc.) (Toole et al., 2000). It was documented that ship shadowing was avoided. Data in the upper 12 m were used to extrapolate the radiances and irradiances to data just below the surface (Kostadinov et al., 2007). Remote sensing reflectance just below the surface [$R_{rs}(0^-,\lambda)$], the product provided to this research, was obtained as a computation of (Kostadinov et al., 2007):

$$R_{rs}(0^-,\lambda) = \frac{L_u(0^-,\lambda)}{E_d(0^-,\lambda)} \quad (1)$$

Where λ refers to wavelength.

Surface chlorophyll *a* concentrations were obtained by fluorometry from Niskin bottle samples (Strickland and Parsons, 1972; Kostadinov et al., 2007). Absorption spectra (absorption by detritus - a_d , organic matter – a_g , and total particulates - a_p) were obtained with a Shimadzu UV2401-PC spectrophotometer, from 400 to 700 nm, in 2 nm increments. Further details on the PRR-600 characteristics and on how the different absorption fractions were collected and handled in laboratory can be found in Toole et al (2000) and Kostadinov et al (2007), respectively.

Linear interpolation was performed to estimate the absorption values for intermediate values when necessary. The data was also extrapolated to 870 nm by assuming constant absorption after 700 nm (Gilerson et al., 2008). Absorption by phytoplankton (a_{ph}) for the necessary wavelengths was calculated by subtracting the absorption by detritus from the absorption by total particulates, following Mueller et al (2003a) and Kostadinov et al (2007).

The cruises and stations' IDS as provided by The Plumes and Blooms Project will be maintained throughout this M.Sc.

3.4. Conversions and data-preparation

Through this M.Sc., some conversions and data transformations were needed in order to fit the purpose of comparing same units/quantities, or to fulfil model requirements. Here it is a list of the transformations performed and the methods used for such, for consultation along the reading. Some definitions can also be found in Appendix III.

From L1B to top-of-atmosphere radiance

- *MERIS*

Level 1B MERIS data consists of calibrated and scaled top of atmosphere radiances (L_{TOA}). Because the data is scaled, the term L_{TOA} must be multiplied by a factor that varies for each wavelength, specific for each image, and that can be found in the MERIS metadata (in the GADS – Global Annotation Datasets). Using BEAM, however, the values are automatically scaled when correction for the Smile Effect is performed. This correction is a standard procedure recommended by ESA and Bourg et al (2008) and it refers to small-scale variations of the central spectral wavelength of each pixel, which need to be compensated. Important to state that BEAM, the standard software to process ENVISAT sensors like MERIS, was considered the best alternative for such correction, and neither the correction's efficiency nor the methodology used were further questioned.

- *MODIS*

MODIS L1B data is organized as 16-bit unsigned integers (Scaled Integer – SI). In order to retrieve top-of-atmosphere radiance data, the following formula is applied (wavelength dependent – λ) (Toller et al., 2006):

*Radiance (λ) = radiance scale (λ) * (SI – radiance offset)*

The terms are found in the MODIS metadata, for each of the desired wavelengths (easily retrieved using the HDFView toolbox).

From radiance to reflectance

In order to reduce "in between scene variability", i.e. reducing the influences of incoming solar radiation, sensor zenith angle and water composition, the spectral radiance can be converted into reflectance by accounting for solar irradiance, through the general formula (Robinson, 1985; Peijuan et al., 2003):

$$R_{TOA}(\lambda) = \frac{\pi L_{TOA}(\lambda)}{F_0(\lambda)\cos(\theta)} \tag{2}$$

With

$F_0(\lambda) = [F_0(\lambda)] * (1/d)^2$

Where

$[F_0(\lambda)]$ = Mean extraterrestrial solar irradiance per wavelength, in mW/m^2;

d = Earth-Sun distance at time of measurement, measured in astronomical units;

R_{TOA} is the unitless top-of-atmosphere reflectance; L_{TOA} is the measured radiance in mW/m^2 sr; F_0 is the extraterrestrial solar irradiance corrected for each day of the year (through the equation that accounts for the Earth-Sun distance) measured in mW/m^2. All three parameters are wavelength-specific (λ). θ refers to the solar zenith angle in degrees for each pixel, which for MODIS is obtained as a product in the Level 2 data (available for download at http://oceancolor.gsfc.nasa.gov/), while for MERIS it is a standard band in the Level 1 dataset itself.

Considering values for the mean extraterrestrial solar irradiance is of concern in the ocean colour community. Up to this moment, sensors have been internally calibrated assuming diverse reference bodies and $[F_0(\lambda)]$ values, which makes direct comparison an extra challenge (Morel and Mueller, 2003). Luckily in this case, MODIS and MERIS share a common scale for the extraterrestrial solar irradiance, that of Thuillier et al (2003), available for consultation at http://www.ioccg.org/groups/mueller.html in 1nm increments. Intermediate values for the sensor's specific wavelength were estimated through linear interpolation.

Earth-Sun distances at date of image acquisition were obtained from NASA's Jet Propulsion Laboratory website, http://ssd.jpl.nasa.gov/horizons.cgi#top.

From top of atmosphere reflectance (R_{TOA}) to remote sensing reflectance (R_{rs})

From remote sensing reflectance it is understood the reflectance obtained after removing the effects of the atmosphere, sunglint and white caps on the water surface, i.e. after atmospheric correction. The transformation was also performed because R_{rs} tends to be a standard input to many of the ocean colour algorithms. Transforming R_{TOA} into R_{rs} requires dividing R_{TOA} by π, a factor considered sufficient to convert irradiance into radiance in a Lambertian environment (Feldman and McClain, 2007a). R_{rs} is measured in *sr* (steradians).

From below water reflectance [$R_{rs}(0^-)$] to above-water reflectance [$R_{rs}(0^+)$]

Assuming a flat surface, accounting for the transmission through the air-sea interface, i.e. converting between below water reflectance and above water reflectance, requires the following (Mobley, 1994):

$$R_{rs}(0^+) = R_{rs}(0^-) * 0.54 \quad (3)$$

This transformation was used in two situations:

- to convert below-water reflectance in situ measurements provided by the University of Santa Barbara (claimed to have resulted from the extrapolation of sub-surface measurements) to above-water reflectance;
- to convert above-water reflectance to below-water reflectance as a requirement for the inversion calculations of Gordon et al (1988).

Match-ups

MODIS and MERIS R_{TOA} spectra matchups represented the average of a 3x3 pixels window centred around the position of each field measurement, following recommendation of the International Ocean Colour Protocol (Mueller et al., 2003b).

Surface Projection

Both MODIS and MERIS imagery were projected to Geographical lat/long coordinates, datum WGS84, in early stages of processing, within BEAM (MERIS) and ENVI (MODIS) environment. The re-sampling method used was nearest neighbour, as it is a computationally efficient option that preserves the original range of pixel values (Longley et al., 2007). For MODIS images, the option “correct for bow-tie effect” was activated. This effect is known to cause distortion over the edges of the images and needs to be corrected (Wen, 2008).

3.5. Atmospheric Correction

As very clearly stated by Antoine and Morel (2005),

> *"When an ocean-colour sensor measures the radiance backscattered by the ocean-atmosphere system, it receives in the visible part of the spectrum a signal that is largely dominated by the 'atmospheric path radiance'. This radiance originates from photons scattered by air molecules and/or aerosols, which can also have been reflected at the sea surface, but have never penetrated the ocean".*

Because this atmospheric contribution can be responsible for more than 90% of the signal received by the sensor in the visible domain, its effect needs to be removed for a more accurate estimation of water leaving radiances, which carry information on the bio-optical characteristics of the oceanic surface waters (Antoine and Morel, 1999). The process of retrieving water-leaving radiances from total radiance is known as atmospheric correction (Antoine and Morel, 1999). It is a key procedure in the ocean colour remote sensing, as well as one of the most delicate steps of data processing and preparation (Yang et al., 2007). Diverse techniques are used to account for that, and different approaches often lead to different results. Not only the methodology, but corrections over coastal waters alone have proved to be a challenge. That's because the majority of the atmospheric correction algorithms developed rely on assuming zero reflectance in the near-infrared, which is not the case in complex waters with various constituents influencing ocean colour (Ruddick et al., 2000). Many techniques have been developed to try to overcome this issue, and many of those are sensor-specific, for example: for MODIS Case-II waters, the one of Wang and Shi (2007). For SeaWiFS, the one of Ruddick et al (2000), Hu et al (2000) and Li (2003). For MERIS Case-II waters, the technique developed by Antoine and Morel (1999); amongst many others.

In the case of merging radiometric units from different sensors, differences in atmospheric correction schemes can be considered as the greatest contributor to uncertainties in the generated outputs (IOCCG, 2007; Mélin et al., 2007). Therefore, in order to increase the potentiality of MODIS and MERIS' inter-relation, the same atmospheric correction scheme will be applied to both, following recommendation of Maritorena and Siegel (2005).

Radiative transfer models, and in this case, the Second Simulation of the Satellite Signal in the Solar Spectrum (6S) (Vermote et al., 1997), was considered a reliable option. By assuming that the radiances related to the atmospheric signal can be decoupled into specific scattering and absorption compartments, and being molecular scattering and gas absorption satisfactorily estimated for a certain point in the Earth, a final atmospheric contribution would only depend on retrieving the contribution of aerosol (Trishchenko et al., 2002; Antoine and Morel, 2005). Aerosol concentration in the atmosphere, however, vary rapidly in time and space, and in situ values are not abundant and readily available, which would require testing the model for diverse aerosol concentrations (Yang et al., 2007). For 6S is a pixel-based radiative transfer model, finding the best combination of inputs for every pixel in a desired area proved to be time consuming. After not being able to get sensible results (while plotting the corrected spectra against the field measurements, great deviations from the expected value as well as negative reflectances were observed – results not shown), an alternative method was selected.

The chosen atmospheric correction procedure then relies on one of the most important assumptions sustaining this M.Sc.: field measurements are considered the best possible approximation of the water's optical properties, and any of the two sensors should be able to estimate the values observed in the field. Any deviation from that measurement would mean an error, amongst which atmospheric interferences are considered a great part of. Based on the latter argument, atmospheric contribution for every wavelength was assessed in a straight-forward manner:

Where $R_{TOA}(\lambda)$ is the top-of-atmosphere reflectance for every wavelength obtained with Equation 2, for each sensor,

$$R_{TOA}(\lambda)_{\text{MERIS}} - R_{TOA}(\lambda)_{\text{field}} = \text{atmospheric contribution}_{\text{MERIS}}(\lambda) \qquad (04)$$
$$R_{TOA}(\lambda)_{\text{MODIS}} - R_{TOA}(\lambda)_{\text{field}} = \text{atmospheric contribution}_{\text{MODIS}}(\lambda)$$

Intuitively, by subtracting the resulting factor (atmospheric contribution) from the original remotely sensed data, atmospherically corrected reflectance is generated. For MODIS and MERIS separately, one point for each date was selected to generate the factor that would correct all other points in that specific date. The candidate point should be located around the centre of the available points, and not be contaminated by land pixels, or negative reflectances. The points that simultaneously satisfied these requirements for all cruises were Point 5 for the first four cruises, and Point 2 for the last cruise (as only three measurements were available for this date - Points 3, 2 and 1). The atmosphere was considered homogeneous throughout the study area. Choosing a reference point to correct the images, as opposed to using all available matchups or their mean, represented an attempt to preserve data independency, allowing the extra pairs to be used for validation.

If this process was considered as described in this stage, however, only a limited number of wavelengths could be directly corrected, because wavelength-matchups between sensor and field data are limited: 443 nm for MODIS, and 490 and 510 nm for MERIS. In order to allow the correction of all wavelengths of both sensors, a bio-optical model was used to estimate field measurements for the "unknown" wavelengths, as explained later on (Page 22). For the common wavelengths, the average between the modelled spectra generated and the original field data for each sensor was taken. The result was then used to atmospherically correct the full spectra from MODIS and MERIS.

3.6. Reflectance model and Bio-optical model

> *"A reflectance model, run in the forward direction, predicts spectral reflectances given constituent concentrations and other properties of the in-water constituents. The bio-optical algorithm is the inverse of the reflectance model. That is, it predicts constituency concentrations and their optical properties given spectral reflectances derived from atmospherically corrected satellite observations". (Campbell, 1996)*

Remote sensing reflectances just above the sea surface [$R_{rs}(0^+,\lambda)$] are apparent optical properties (AOP), which by definition vary according to the water constituents (i.e. IOPs), weather conditions and geometric angles of sun and satellite (Preisendorfer, 1960; Mobley, 1994). Considering that the IOPs absorption and backscattering can be measured or estimated, a first-order model relating R_{rs} to the water constituents follows (Gordon et al., 1975; Mobley, 1994):

$$R_{rs}(0^+,\lambda) = k\left(\frac{f}{Q}\right)\left(\frac{b_b(\lambda)}{b_b(\lambda)+a(\lambda)}\right) \tag{5}$$

Where a and b_b are the absorption and backscattering coefficients, respectively, varying in time and space. All other variables are considered invariant. The factor

f/Q[1] was assumed to be independent of wavelength and solar zenith angle for oceanic waters, and equal to 0.0949 (Gordon et al., 1988; Tzortziou et al., 2007). Important to notice that for Case-II waters the appropriate value for the factor remains unknown (Tzortziou et al., 2007); k is the factor accounting for the transmission and reflection of the sea-air interface when converting above-water reflectance into below-water reflectance, equal to 0.54 (Mobley, 1994).

The same equation described above can be re-written in a quadratic form, by the addition of a second-order term (Gordon et al., 1988):

$$R_{rs}(0^+,\lambda) = k\left(\frac{f}{Q}\right) g_1\left(\frac{b_b(\lambda)}{b_b(\lambda)+a(\lambda)}\right)\left[g_2\left(\frac{b_b(\lambda)}{b_b(\lambda)+a(\lambda)}\right)\right]^2 \qquad (6)$$

Where g_1 can be related to the f/Q factor cited above, and g_2 is equal to 0.0794 (Gordon et al., 1975; Gordon et al., 1988).

In practical terms, total absorption and backscattering coefficients (a and b_b) are considered as such:

$a(\lambda) = a_w(\lambda) + a_{ph}(\lambda) + a_{cdm}(\lambda)$
$b_b(\lambda) = b_{bw}(\lambda) + b_{bp}(\lambda)$

Where the subscripts *w, ph, cdm and p* represent water, phytoplankton, detritus and CDOM combined, and particles, respectively.

a_w and b_{bw} have known distribution along the spectrum. The a_w values considered are the ones from Pope and Fry (1997), while for b_{bw}, Smith and Baker (1978) values were used. When necessary, the values were linearly interpolated to match the wavelengths used in the study. Changes in a_w and b_{bw}'s spectral distributions due to their known dependence on temperature and salinity were not considered in this study (for discussion on the subject, refer to Feldman and McClain (2007b)).

The other elements, a_{ph}, a_{cdm} and b_{bp} are considered to vary assuming specific spectral shapes, which allows the modelling of IOP's for any desired wavelength (which is particularly appealing in this M.Sc.):

[1] f is a complex function of wavelength, IOPs, solar zenith angle, aerosol optical thickness and surface roughness (Gordon et al, 1975; Tzortziou, 2007). Q is the ratio of upwelling irradiance to upwelling radiance $Q = E_u(\lambda)/L_u(\lambda)$ (Austin, 1974).

$$a_{ph}(\lambda) = Chla^{*}_{ph}(\lambda) \tag{7}$$

$$a_{cdm}(\lambda) = CDMe^{-S(\lambda-\lambda_0)} \tag{8}$$

$$b_{bw}(\lambda) = BBP(\lambda/\lambda_0)^{-\eta} \tag{9}$$

where Chl is the chlorophyll *a* concentration in mg/m^3, a^*_{ph} is the chlorophyll *a* specific absorption coefficient (considered as an interpolation of the values obtained by Kostadinov et al (2007), which possibly represent the most finely tuned values available for The Santa Barbara Channel region); CDM is the absorption coefficient of CDOM and detritus at a reference wavelength of λ_0 = 443 nm, *S* is the spectral dependency constant for the latter two absorption parameters (calculated through inversion of the ocean colour signal, further shown) (Bissett et al., 2005); BBP is the particulate backscattering coefficient at 443 nm, and *n* is the exponent for particulate backscattering (also calculated by inversion); λ_0 is the reference wavelength, being λ all the other available wavelengths. Considering all the available field data, and running the reflectance model in the inverse direction (characterizing then a bio-optical model) it is possible to estimate chlorophyll *a* from the first equation, CDM from the second, and b_{bp} and BBP for the third.

Estimating IOPs and AOPs as part of the atmospheric correction scheme

As previously explained, the atmospheric correction proposed is wavelength-based, which would require the field measurements to record information on the same bands of MODIS and MERIS. As in situ above-water reflectance was only collected for 5 wavelengths, it was attempted to estimate what the instrument (i.e. PRR-600) could have measured had it had more bands available.

3 steps summarise the process:
1) Inversion of reflectance model to estimate *b* and b_{bp};
2) Estimation of the spectral slope of b_{bp} (η);
3) Forward reflectance model to estimate R_{rs} for extra wavelengths;

1) Provided the variables a_w, a_{ph}, a_{cdm}, b_w were known or measured in the field, the first-order Equation 4 was inversed (i.e. estimating IOPs from remote sensing reflectance spectra – bio-optical model), to solve for the parameter b_b (and consequently $b_{bp,}$ by removing the backscattering of pure water (Morel, 1974)), the only left unknowns:

$$b_b(\lambda) = \frac{R_{rs}(\lambda)a(\lambda)}{kg_1 - R_{rs}(\lambda)} \tag{10}$$

2) Once the particulate backscattering coefficient for all 5 wavelengths was known, the spectral slope of b_{bp} for each wavelength could be estimated, using the 443 nm band as the reference one (λ_0):

$$\eta = -\left[\ln\left(\frac{b_{bp}(\lambda)}{b_{bp}(\lambda_0)}\right)\right]\left[\ln\left(\frac{\lambda_0}{\lambda}\right)\right] \tag{11}$$

For each date, an average of the resulting spectral slopes was taken, in order to represent η at reference wavelength 443 nm. It is important to notice that fixed values for both b_{bp} and a_{cdm} slopes, are usually used by the scientific community (consult Maritorena et al, 2002; Kostadinov et al, 2007). b_{bp} and η, however, are considered to be highly variable in time and space, and it is likely that using one constant value for a set of data points can introduce errors in any retrieved IOPs and AOPs (Kostadinov et al, 2007). Kostadinov et al (2007) published slope values specifically for the Santa Barbara Channel region, after modelling nearly 8 years of data. Considering the small number of sampling units available for this study (5 cruises with 7 points each, spread over 4 years) and their high optical variability, however, it was decided to generate point-specific η values.

3) Having estimated all unknown elements of the formula, and using the average backscattering slope showed above as a constant, the two-parameter Equation 5 can then be easily solved, in the forward mode (i.e. remote sensing reflectances are estimated, as opposed to IOP's – *reflectance model*) for all desired wavelengths, in this case, all the wavelengths covered by MODIS and MERIS: 21 in total. It is important to notice that all calculations presented here were executed using Microsoft Excel. Therefore, it was for matters of simplicity that the inversion was performed using the one-order equation. It is clear that Equation 4 could have been used in the forward mode as well, but once Equation 5 considers more factors and its execution in the forward mode is just as simple, the latter equation was used.

After these procedures, field spectra will have data corresponding to each of MERIS and MODIS' wavelengths. A model tuning can be performed for the common original wavelengths (443, 490 and 510 nm) – simple average. That is an attempt to preserve the initial field values. After that, the atmospheric correction can be executed, as shown back in Page 19.

3.7. Expanding MODIS and MERIS spectra

Once the role of bio-optical models in estimating remote sensing reflectances for extra wavelengths was explained, performing the spectral merging proposed in this M.Sc. is a straight-forward process. After atmospheric correction, any sampling points with negative or suspicious reflectance values; any points with no respective pair in the other sensor; and the points utilised to perform the atmospheric correction itself (Points 5 and 2) were removed. The resulting 15 spectra per sensor (representing 6 points in space and 5 dates, but not every cruise sampled every station) were embedded in Equation 4, in order to estimate backscattering coefficients and slope for each point. Important to note that the reference wavelength used for MODIS was 443 nm, while for MERIS it was 442.5 nm. After that, having estimated all the necessary variables, Equation 5 was used to determine remote sensing reflectances for all wavelengths of MODIS and MERIS combined, finally resulting in 15 pairs of spectra (15 for MODIS and 15 for MERIS) with 21 wavelengths each. The same was done for the field observations.

3.7.1. Spectral Merging

This M.Sc. tried to corroborate the assumption that, by multiplying MODIS and MERIS' estimations by a certain wavelength-dependent factor, the two sensors could more successfully predict the observed values in the field, in a way that:

$$(\alpha)\, R_{rs}(\lambda)\mathrm{MODIS} + (\beta)\, R_{rs}(\lambda)\mathrm{MERIS} + \mathrm{Constant} = \mathrm{FIELD}\ R_{rs}(\lambda) \qquad (12)$$

The terms α and β were assumed to vary for every wavelength, in such a way that different corrections should be applied in different parts of the spectrum in order to improve the accuracy between field and remote sensing measurements.

Eight out of the fifteen corresponding spectra of MODIS, MERIS and field measurements were selected to test the above relationship. The factors α and β were estimated through multi-linear regression for each of the 21 wavelengths, using STATISTICA v.6.0. MODIS and MERIS were considered independent variables. To sustain the assumption, the processing method used was "Backward Regression", which first tests the impact of the two independent variables together in explaining the dependent variable (field data). In case one of the coefficients α or β is insignificant[2], it is eliminated and the regression is re-run for the other variable, testing if the removal improved the overall regression results (observing p-value[3], R^2 and [4]adjusted R^2). It is important to keep in mind that in regression with multiple independent variables, each coefficient indicates "how much the dependent variable is expected to increase when that independent variable increases by one, holding all the other independent variables constant" (Princeton-University, 2008).

STATISTICA provides as final result the setting (α and β, only α or only β) that best explains the dependent variable. A significance level of 95% (α=0.05) was set for the entire analysis. All intercept values (constants) were maintained in the regression equations even when not significant, as their removal can jeopardise the overall regression. Regarding the interpretation of the results obtained, however, care was taken when analysing each "level of significance", as even though an output may seem statistically insignificant, the "practical importance" of the result may play an important role, depending on the goals of the study (Moore and McCabe, 1998). Much of that may be related to the fact that, in some occasions, MERIS and MODIS' measurements can co-vary as they are essentially measuring the same water, which statistically indicates colinearity, an artefact that is usually encouraged to have removed from regression analysis. This M.Sc., however, assumes that this colinearity can in fact help better predict the real environment.

The seven spectra left aside were used for validating the coefficients found, and plotted against the expected values in the field for comparison. Root-mean square error (RMSE) was the basic tool used to investigate how the merging improved or not the estimation of real values. It is given by (Longley et al., 2007):

$$RMSE = \sqrt{\frac{\sum(\text{modeled - observed})^2}{\text{n}}} \tag{13}$$

[2] In statistics, the term significance is used to indicate if there is evidence against the null hypothesis at a certain level of significance (α), which is a fixed value considered as decisive. For the purposes of this study, the null hypothesis could be that including the coefficient (s) in the regression does not improve the accuracy of field estimations (Moore and McCabe, 1998).
[3] P-value is the smallest level α at which the data are significant. The smaller the p-value, the stronger the evidence against the null hypothesis provided by the data. Low significance level does not mean there is a strong association, only that there is strong evidence of some association (Moore and McCabe, 1998).
[4] R^2 and Adjusted R^2: R^2 is the proportion of the variation of the dependent variable that is explained by the independent variables (Moore and McCabe, 1998). The adjusted R^2 takes into consideration the degrees of freedom of the data, and is specially used in multiple regression analysis.

4. Results

4.1. Pre-processing of MODIS and MERIS data

R_{TOA} products generated for the locations where in situ measurements were available (28 points), for the spectrum range 412.5 – 869.5 nm for MODIS, and 412.5 – 865 nm for MERIS, as shown in Figure 2 (a and b).

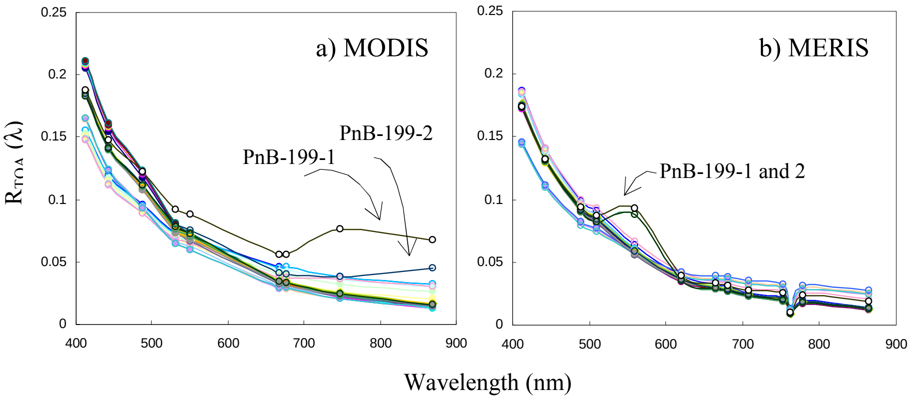

Figure 2 a) Top of atmosphere reflectance (R_{TOA}) calculated for 28 measurements representing 5 dates and 7 locations in space from the Plumes and Blooms dataset, for the 9 individual MODIS wavelengths (not every cruise sampled 7 stations). Each line represents one location in time. The points were joined together through a line only to facilitate the separation among the available spectra. Figure 2b) Same as a), but in this case for all 13 MERIS' wavelengths.

For MERIS, interesting to note the behaviour of the oxygen absorption band at 761.875 nm for all points, which presents small variance in the reflectance measured. Two spectra vary considerably from the others for both sensors, but in different parts of the spectrum. Those points are highlighted in the graphs, and correspond to Points 1 and 2 for December 2007 – PnB 199 (Refer to Chapter 2 for the sampling location). For MERIS, the exceeding values occur for band 560 nm, while for MODIS they are noticed all through near infrared. Apart from those, the range of reflectance values registered by each sensor is comparable.

4.2. Field Data

The 28 available field measurements, already converted from $R_{rs}(0^-)$ to $R_{rs}(0^+)$, for the wavelengths 412, 443, 490, 510 and 555 nm are shown in Figure 3.

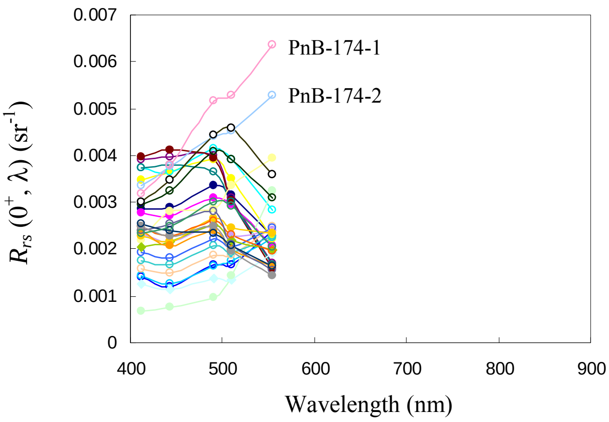

Figure 3 Spectra collected in the field, for 5 wavelengths. The extended x axis is set as such to show the amount of information missing from field measurements, and that will need to be estimated to make them comparable with the data registered by the sensors. 28 sampling points are included in the graph, representing 5 different dates. One point for each date was chosen to perform the atmospheric correction of MERIS and MODIS.

The high variance between all points is apparent, especially when they are located near the coast. Highlighted in the graph are two of those examples: points 1 and 2 from PnB-174. A point for each date was selected to perform the atmospheric correction of the remote sensing data: point 5 for cruises PnB-142, 174, 184 and 189, and point 2 for PnB-199.

4.3. Atmospheric correction

Part 1) Applying bio-optical model to obtain η and b_{bp} (λ_0)

Backscattering slope η and b_{bp} for the five points selected for atmospheric correction were estimated through inversion of Equation 4, and the results follow in Table 4:

Table 4 Average spectral slope of suspended particulate matter and backscattering coefficient at the reference wavelength of 443 nm for each selected point.

Station	(η) average all 5 bands	(b_{bp}) at 443 nm*
PnB 142 - 5	2.974395	0.010555
PnB 174 - 5	2.546528	0.009869
PnB 184 - 5	2.648507	0.016215
PnB 189 - 5	3.588411	0.005432
PnB 199 - 2	2.093362	0.010628

* b_{bp} was generated for all 5 bands. Only the 443 nm is shown because that was the b_{bp}-base used to estimate b_b and therefore R_{rs} for all other bands in the forward mode.

Part 2) Applying a reflectance model to estimate field R_{rs} for MODIS and MERIS' wavelengths

The values of η and b_{bp} (Table 4) were used in Equation 5 (Page 21), to generate spectra for the same wavelengths as of those of the sensors. Only bands 443 nm for MODIS and 490 and 510 nm for MERIS could be directly validated, as they were the only common bands, and the relative error of the estimation follows in Table 5:

Table 5 Difference between the observed value in the field and the value obtained after applying the inverse and forward models, for the 5 points chosen to perform atmospheric correction of MODIS and MERIS images. Only common bands between field observations and MODIS / MERIS are shown. Relative error (RE), is given in %.

Station	Wavelength (nm)	R_{rs} (field)	R_{rs} estimated (modelled)	RE (%) of estimation
PnB 142-5	443	0.003645	0.003662	0.464227
	490	0.003922	0.003872	1.291322
	510	0.003498	0.003804	8.044164
PnB 174-5	443	0.001126	0.001128	0.177305
	490	0.001365	0.00139	1.798561
	510	0.001349	0.001554	13.19176
PnB 184-5	443	0.001822	0.001827	0.273673
	490	0.002225	0.002082	6.868396
	510	0.002045	0.002419	15.46093
PnB 189-5	443	0.002084	0.002089	0.239349
	490	0.002388	0.002292	4.188482
	510	0.001969	0.002463	20.05684
PnB 199-2	443	0.003226	0.003239	0.401358
	490	0.00408	0.003867	5.508146
	510	0.003895	0.004088	4.721135

It is apparent from Table 5 that relative errors between modelled and estimated R_{rs} values increase with increasing wavelength. In all but the last station, estimation for wavelength 510 nm performs more poorly than the others. Errors for estimations in band 443 nm are relatively small and constant, i.e. between 0.17 and 0.46 % for all stations. Observing RE at this stage is important as it provides an idea of the error propagation of all steps involved before spectral merging, which can influence the final output. Important to remember that the final value used to represent each of the above wavelengths was an average of the initial R_{rs} from the field and the R_{rs} modelled.

After performing atmospheric correction (i.e. subtracting the reflectance spectra from MODIS and MERIS by the spectra from the central points selected for atmospheric correction, as in Equation 4, page 19), some points were excluded as they failed the procedure adopted (i.e. resulted in negative values). A summary of the initial and final data available for use in the different parts of the M.Sc. is shown in Table 6.

Table 6 Summary of data available as provided within the Plumes and Blooms Experiment, used for atmospheric correction, available after atmospheric correction, and the points used for calibration or validation of the merging procedure. For information on the sampling locations, refer back to Chapter 2.

Cruise #	Date	Provided data (PnB point #)	Point used for AC	Points available after AC*	Point used for calibration	Points used for validation
PnB-142	15/01/2003	7, 6, 5, 4, 3, 2, 1	5	7, 6[1], 4, 3, 2, 1	6, 4, 2	7, 3, 1
PnB-174	21/06/2005	7, 6, 5, 4, 3, 2, 1	5	7, 6	6	7
PnB-184	21/03/2006	7, 6, 5, 4	5	4[2]		4
PnB-189	15/11/2006	7, 6, 5, 4, 3, 2, 1	5	7, 6, 4[3], 3[4], 2[5]	7, 6, 4	3, 2
PnB-199	11/12/2007	3, 2, 1	2	3[6]	3	

*Observation: in some cases, only a few bands failed the atmospheric correction (negative values), in which case those bands were removed from the analysis:

[1] band 869.5 nm for MODIS

[2, 4,5] bands 667 onwards for MODIS

[3] band 748 nm onwards for MODIS

[6] band 753.75 onwards for MERIS

That procedure was considered in order to avoid lack of data for further analysis (presuming reliable quality). Points used for atmospheric correction were automatically made unavailable.

Atmospheric correction for Points 3, 2 and 1 for MODIS, in PnB-174 resulted in negative reflectances for most bands, and were directly excluded from the dataset. Those points are the same ones highlighted in Figure 3. Likewise, near-infrared values for point 1 in PnB-199 for both MODIS and MERIS were increasingly higher towards the end of the spectrum, reaching 2% at around 870 nm. Those values are suspicious, as even in extremely turbid environments reflectances in the near infra-red do not exceed 0.5%, due to the fact that water is a strongly absorber at those wavelengths (IOCCG, 2000). Therefore, those points were also excluded from the analysis. Those are the same points highlighted in Figure 3.

The spectra (points) successfully corrected for the atmospheric effects, i.e. which resulted in above-zero R_{rs} in the same order of magnitude as other measurements for the same date, for each sensor, is shown in Figure 4 (a and b).

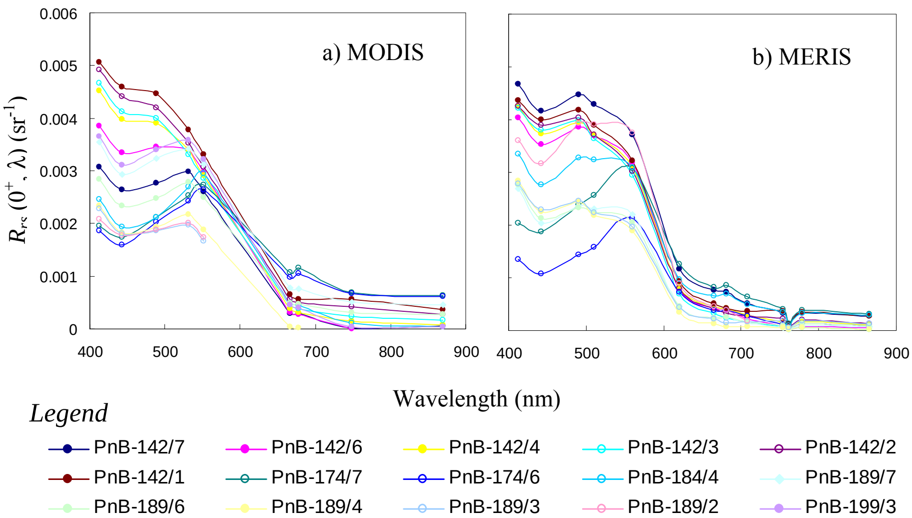

Figure 4 Above-water remote sensing reflectance spectra for MODIS (a) and MERIS (b) datasets obtained after atmospheric correction procedures. Points that have failed the atmospheric correction were not included. In case only certain parts of the spectrum failed, those points were included for the wavelengths with good-quality retrievals. Different colours refer to different stations.

In general, a primary peak occurs for both sensors at around 550 nm. Secondary peaks at around 680 nm can be depicted for both MODIS and MERIS data, for the cruises/stations: PnB-174 / 7 and 6, and PnB-189 / 7. MERIS' dataset also points out a peak for cruise PnB-142 / 7. In general, MERIS values appear higher than those same points registered by MODIS. The oxygen absorption feature at 761 nm for MERIS is apparent for all points analysed. The means and standard deviations presented in Figure 5, which considers the all dates/stations as whole, provide clearer comparison between both sensors:

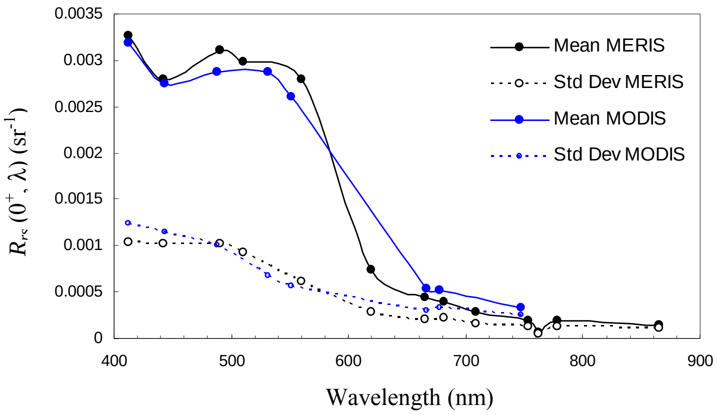

Figure 5 Overall mean and standard deviation for all MODIS and MERIS' spectra and available wavelengths of each sensor. It is clear that the continuous line here presented is not a realistic approach to form the spectrum, but it was chosen to improve visualisation of the spectral shapes.

Throughout the spectrum and when compared to MERIS, MODIS shows lower R_{rs} values in the blue-green regions, and higher reflectances in the red-near infrared regions, which present always non-zero signals. Variability of R_{rs} is at its largest at 412 nm, but just as high near 440 nm. The similarity between the mean and standard deviation spectrum shape is not strong, and at least for the available wavelengths the latter is always smaller than the mean. The previously observed peaks at around 685 nm are smoothed out when means are considered. For the first two estimations, 412.5 and 442/443 nm, a good agreement between both sensors is indicated.

To illustrate the similarity between MODIS and MERIS data, R^2 values for the band combinations 412.5/412.5, 443/442.5, 667/665 are, respectively: 0.7767, 0.7471, and 0.2155.

4.4. Expanding MODIS and MERIS spectra to all available points

Just like the first steps for atmospheric correction, i.e. to obtain η and b_{bp} values for the five selected points and then use those to estimate R_{rs} for determined wavelengths, now all 15 successfully atmospherically corrected spectra for each sensor and the correspondent field measurements were used in inversion models to estimate η and b_{bp} at 443 nm. The specific results for each station are not shown here to avoid overloading. Overall, the basic statistics for the variables generated are shown in Table 7:

Table 7 Overall mean and standard deviation for spectral slope of suspended matter and particulate backscattering at reference wavelength 443 nm for measurements collected in the field and by MODIS, and 442.5 nm by MERIS, for all 15 available points.

	Field		MODIS		MERIS	
	Mean	Std. dev	Mean	Std. dev	Mean	Std. dev
η per point	2.789036	0.609286	2.277833198	0.508339252	2.043209	0.675298
$b_{bp}(\lambda_0)$	0.007036	0.002203	0.008207173	0.003938717	0.007914	0.003334

Regarding η values, MERIS presents the lowest overall mean, and at the same time the highest standard deviations from the mean. In relation to the backscattering coefficients retrieved, MERIS and MODIS' means and standard deviations vary considerably from that obtained when inverting field measurements.

η and b_{bp} at the reference wavelengths 443 nm for MODIS and 442.5 nm for MERIS were used to estimate particle backscattering coefficients (b_{bp}) for the 21 desired wavelengths of field, MODIS and MERIS (discrete wavelengths of MODIS and MERIS together, as shown in Table 1, Page 4). The results are shown in Figure 6 (a to c). Once b_{bp} is known, and the absorption coefficients were provided within the PnB Dataset (total absorption and absorption by phytoplankton are shown in Figure 6 d and e), R_{rs} for the same wavelengths can be estimated. The spectra for MODIS, MERIS and field, now with all 21 matching wavelengths, are represented in Figure 7 (a to c).

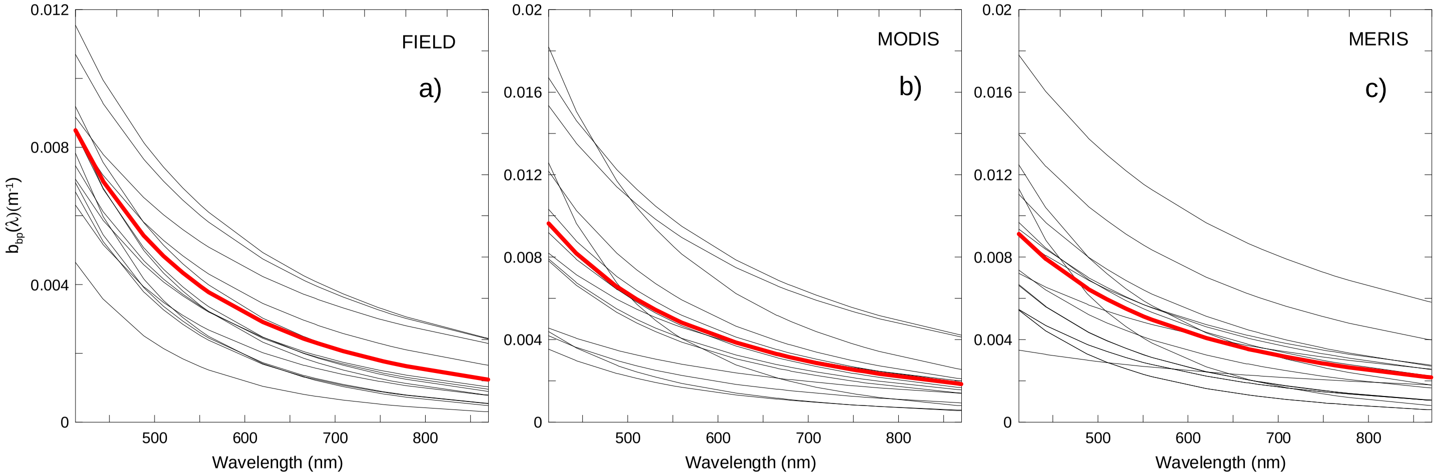

Figure 6 a-c shows the backscattering coefficient b_{bp} estimated in the forward model, for all desired wavelengths, given as inputs the spectral slope η and the b_{bp} from the previous steps. In red, the mean spectra. Figure 5 d) shows the total absorption (*a*) spectra for the same wavelengths, as provided within the PnB dataset. Figure 5 e) shows the absorption by phytoplankton (a_{oh}) only.

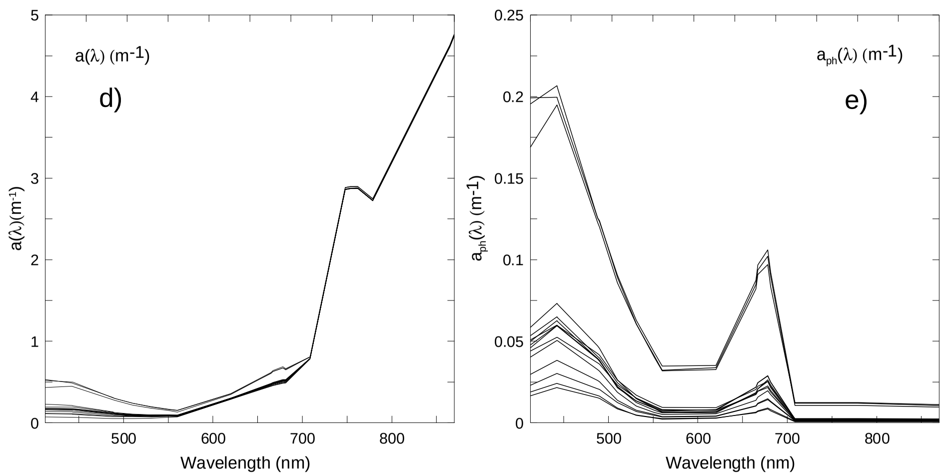

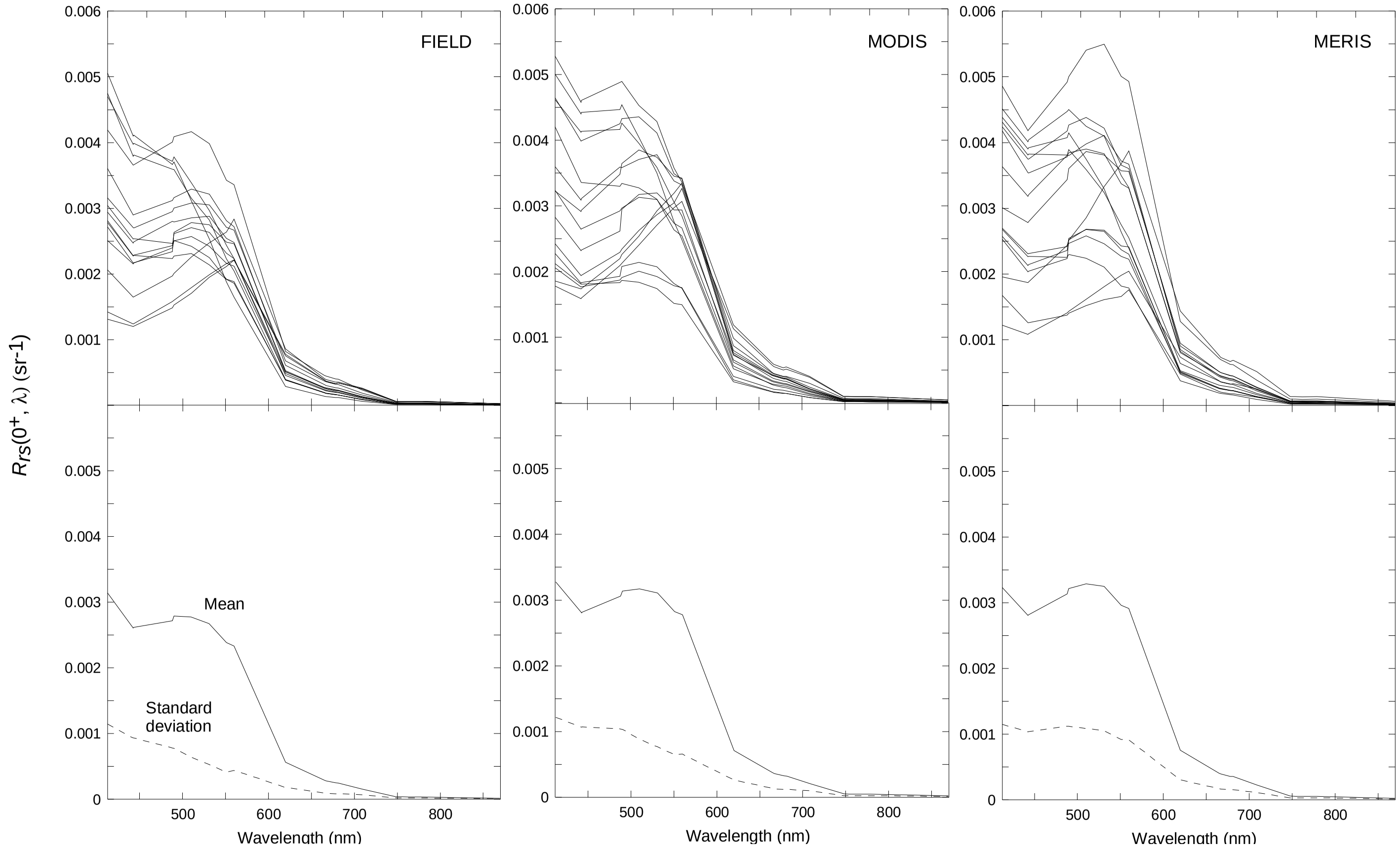

Figure 7 a-c) Based on the b_{bp} and a showed in Figure 5, R_{rs} spectra in 21 wavelengths were generated to express the field, MODIS and MERIS' behaviour. 15 stations are represented. Below each figure, the mean and standard deviation of R_{rs} estimations altogether.

Field b_{bp} estimations seem more homogeneous if compared with the sensor's estimations. MODIS and MERIS' b_{bp} present comparable amplitude of values throughout the spectrum. Estimations of R_{rs} in the blue part of the spectrum, for all three data sources seem relatively high if compared to the subsequent measurements along the spectrum. Field mean spectra presents lower values, followed by MODIS and then MERIS. MODIS and MERIS show similar mean spectral shape, with higher values around 550 nm for MERIS. To some extent, standard deviations of the measurements have similar spectral shape of the mean R_{rs} for MERIS. For field and MODIS, those shapes seem independent of one another.

Relative errors between atmospherically corrected spectra from MODIS and MERIS and the spectra generated through modelling, for the original wavelengths of each sensor (as those are the only ones possible to be compared) are found in Table 8:

Table 8 Relative errors in % representing how the reflectance model performed in returning the values observed after atmospheric correction, for the same bands.

Mean relative error (%) per band (nm)			
MODIS		MERIS	
412.5	3.820966	412.5	4.721014989
443	0.183114	442.5	0.362389033
488	5.123687	490	5.550875496
531	9.318036	510	9.201688982
551	9.444858	560	14.10395371
667	26.09961	620	34.52783603
678	27.73648	665	13.5276065
748	89.72763	681.25	27.14446901
869.5	77.44602	708.75	26.91476601
		753.75	61.02611122
		761.875	50.70051997
		778.75	64.41633012
		865	76.2167282

Small errors in the retrievals of reflectance for wavelength 443 nm and 442.5 nm, the reference bands used in the models for each sensor, are apparent. Similar errors per sensor were observed for bands in the same region of the spectrum, to cite a few, bands 412.5, 488/490, 510/531, 865/869.5 nm. For MODIS, the model performed more poorly when estimating reflectances at 748 nm, while for MERIS the highest relative errors were registered in the 865 nm region. All 15 points were taken into consideration while calculating the errors.

4.5. Spectral Merging

Merging MERIS and MODIS to a unique spectrum consisted in the following:

$$(\alpha)\ R_{rs}(\lambda)\text{MODIS} + (\beta)\ R_{rs}(\lambda)\text{MERIS} + \text{Constant} = \text{FIELD}\ R_{rs}(\lambda)$$

α, β and the constant were obtained via multiple linear regression, which aimed to obtain the necessary factors to estimate the field measurements. Those, together with the basic statistics of the regression analysis for each of the 21 bands, provided by the STATISTICA package, are found in Table 9.

Table 9 Coefficients (α for MODIS, β for MERIS) and intercept (constant) values obtained from 8 calibration points (stations), from multi-linear regression analysis. In blue, the situations where the overall regression was statistically significant. Blank cells mean that the regression resulted in coefficients very close or equal to zero, not improving the overall regression result, therefore being ignored in the final regression model. R^2 was considered when only one variable was included in the model. Adjusted R^2 was considered when both variables were included. Significance level adopted = 0.05.

Wave (nm)	*α*	*p-level*	*β*	*p-level*	*Constant*	*p-level*	*R^2 (Adj. R^2)*	*signif. overall regression*
412.5	1.3488	0.1106	-0.4575	0.5429	-0.00010	0.8693	0.8005	0.0077
442.5	0.7095	0.2243	0.1404	0.7963	1.20E-04	0.8123	0.7960	0.0081
443	0.6999	0.2282	0.1491	0.7833	1.24E-04	0.8074	0.7947	0.0082
488	0.1721	0.6614	0.5216	0.2042	5.71E-04	0.3580	0.6849	0.0240
490	0.1449	0.7118	0.5371	0.1954	6.31E-04	0.3617	0.6362	0.0344
510			0.5692	0.0194	9.68E-04	0.1722	0.6254	0.0194
531			0.4887	0.0522	1.16E-03	0.1429	0.4929	0.0522
551			0.3784	0.1669	1.33E-03	0.1196	0.2919	0.1669
560			0.4012	0.1665	1.22E-03	0.1603	0.2923	0.1665
620	0.2166	0.4556	0.3501	0.4393	1.60E-04	0.5456	0.1792	0.2632
665			0.5420	0.1555	7.95E-05	0.5805	0.3054	0.1555
667			0.5379	0.1588	7.80E-05	0.5767	0.3013	0.1588
678			0.5346	0.1663	6.91E-05	0.5895	0.2925	0.1663
681			0.5469	0.1608	6.41E-05	0.6165	0.2990	0.1608
708	0.2291	0.4378	0.3744	0.4797	2.91E-05	0.7293	0.2554	0.2063
748	0.2227	0.4560	0.3698	0.4991	6.79E-06	0.7522	0.2404	0.2168
753	0.2213	0.4598	0.3686	0.5019	6.65E-06	0.7534	0.2351	0.2206
761	0.2195	0.4648	0.3667	0.5060	6.50E-06	0.7549	0.2277	0.2260
778	0.3571	0.1023			1.86E-05	0.1127	0.3822	0.1023
865	0.3344	0.1237			8.68E-06	0.1235	0.3480	0.1237
869.5	0.3333	0.1247			8.35E-06	0.1240	0.3465	0.1247

The results show that for 10 out of 21 bands, within the 8 calibration points considered, both MODIS and MERIS data contributed more significantly to the overall regression than when the regression was performed for the sensors alone (p-values were more significant). For eight bands, MERIS alone contributed more significantly to the model, and for three bands, MODIS was statistically more efficient. Overall regression performance was only statistically significant (p-value < 0.05) for the first six wavelengths, out of which five received MODIS and MERIS' inputs. Band 531 nm was almost significant at $\alpha = 0.05$ (p=0.0522).

The coefficients for each band were tested to merge MODIS and MERIS spectra of the 7 points (stations) left aside, and the overall performance can be visualised in Figures 8 and 9. Figure 8 focuses on the Root Mean Square Error (RMSE) of each wavelength in relation to the expected "real" value, i.e. the field measurements. Figure 9 focuses on the overall merging performance. The sensor's individual performances are also plotted to check if merging resulted in any improvement in the overall RMSE.

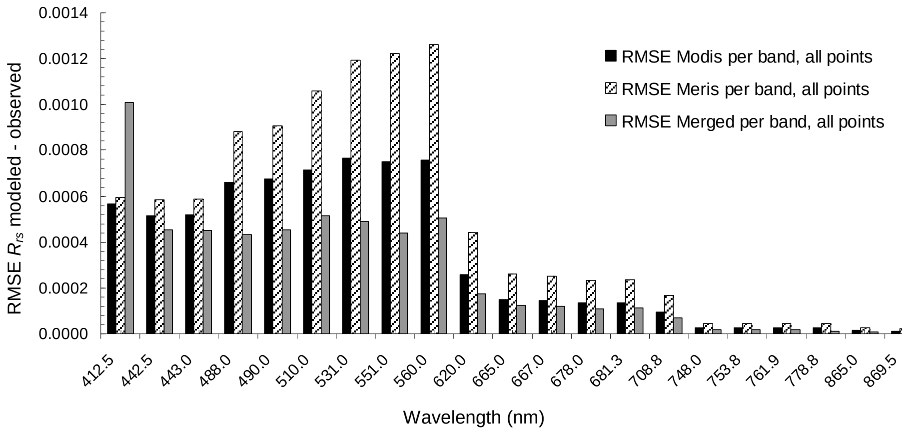

Figure 8 RMSE for each wavelength, considering the sensors alone and their merged result after applying the coefficients β and α. RMSE is in the same units as R_{rs}.

It is apparent from Figure 8 that RMSE is smaller for the merged dataset for all wavelengths except 412.5 nm. Figure 9 reinforces the improvement in the overall fit when the merged data is considered, at the same time that the errors seem to be minimised.

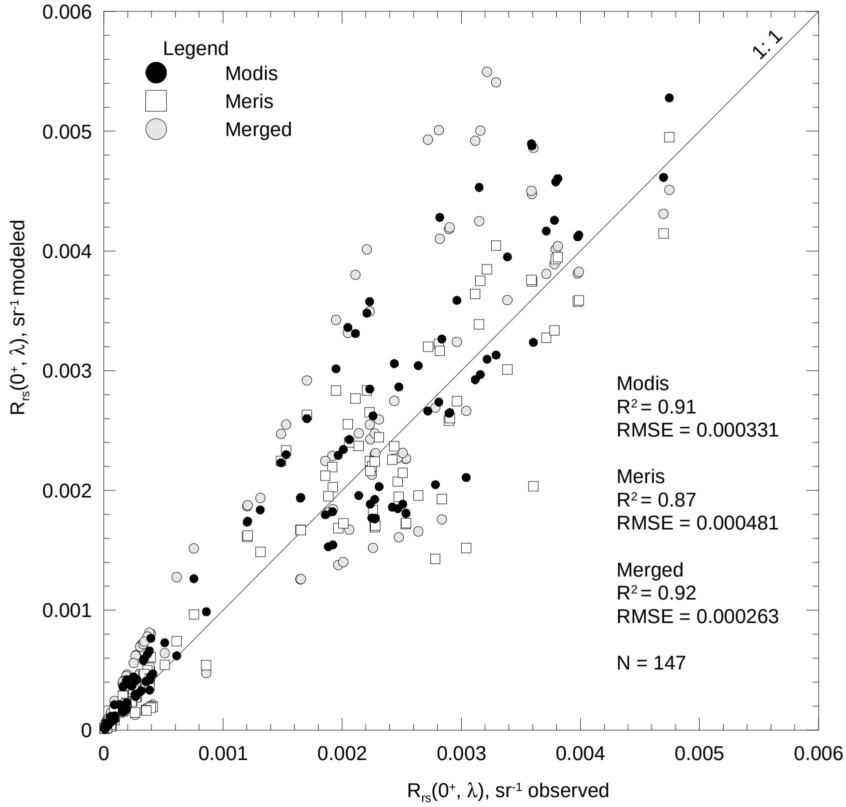

Figure 9 Overall RMSE for all 21 bands of each sensor and for the merged dataset. The continuous line shows the one-to-one relationship.

If, in order to maintain the reliability on the data, the estimations over that wavelength (412.5 nm) are excluded, RMSE from the merged spectra are 0.75 times smaller than MODIS' errors, while MERIS RMSE is at least double of the merged one. More specifically, the new RMSE for MODIS, MERIS and merged data would be: 0.00032, 0.00047 and 0.00022, respectively. R^2 would shift to 0.92, 0.87 and 0.94 for the above sources.

A graphical comparison between the merged spectra and the original field data (before modelling to different bands) and the sensor's original data (atmospherically corrected) are found in Appendix V.

5. Discussion

5.1. Pre-processing of MODIS and MERIS data

The R_{TOA} spectra presented by both sensors have the expected shape for waters contaminated by the atmosphere, i.e. decreasing reflectance along the spectrum and high reflectance in the blue related to high scattering by aerosols and other gases. High reflectance values for points near the coast for PnB-199 (points 1 and 2) may directly indicate high turbidity levels for MERIS, which presents peaks at around 560 nm for those stations. For MODIS, the high values in the near-infrared part of the spectrum for the same points may be an artefact of the spectral averaging method used to extract the radiometric information from the images (averaging 8 pixels around a centre pixel), which may have included pixels very close to the coast, or even shallower water – known to show increased reflectance in the NIR (Maritorena et al., 1994; Cannizzaro and Carder, 2006; Zawada et al., 2007). Some differences between the sensor's retrievals may also be linked to the simple fact that they registered information in different discrete wavelengths, in such a way that had they had the same bands in certain areas (especially around 550 and 560 nm), they could have shown the same spectral features.

Likewise, to some extent, it is possible that the differences in spatial resolution from both sensors may have affected direct comparisons between them during the study. Even though their pixel-based spatial resolution are quite comparable (1km for MODIS and 1.2 km for MERIS), after averaging 8 pixels around a centre point, the issue becomes comparing 9 km^2 of MODIS with 13 km^2 of MERIS. In practice, the spatial averaging can smooth out some features for MERIS at the same time that it can highlight other features such as shallow water and river discharge contribution for MODIS, and vice-versa. To resolve that issue and make retrievals comparable, spatial merging techniques like the ones from Pottier et al (2006) have been developed. That was not, however, the focus of this M.Sc.

Overall, the range of reflectance values registered and calculated for both sensors are comparable, which may indicate that the standardisation of methods when converting TOA Radiance (L_{TOA}) to TOA Reflectance (R_{TOA}) has had a positive effect on making the data as inter-comparable as possible.

5.2. Field Data

It is important to state that the field data used in this study represented the only data to which cloud-free remote sensing images of both MODIS and MERIS were available for the same dates of the cruises in the SBC area.

The high variability of reflectances obtained through PRR-600 for the field measurements likely reflects the environmental, weather and oceanographic transitions and conditions to which the area was subjected to during the period. One set of sampling units from year 2003, one from 2005, two for 2006 and one from 2007 were the basis for performing all the analysis in this M.Sc.

Observing the spectra collected within those years, the large variability around 440 nm shows the importance of the absorption by phytoplankton. Likewise, high values at 555 nm indicates an important role of the backscattering by particles (Toole and Siegel, 2001). That is emphasised when observing points 1 and 2 in PnB-174, which are located closer to the coast and present an elevated signal at around 555 nm, which could be related to a continental runoff contribution. According to the State of California (2007), Department of Water Resources, the month in question presented persistent light rain for the Santa Barbara region, accumulating 25 cm in total, which could have resulted in an increased water runoff and dispersal throughout the coast.

Moreover, divergent currents with different salinity and temperature properties dominate different parts of the SBC, which can also mean that different water masses dominated each of the points, explaining the variability. And because these characteristics also change throughout the seasons, points in the same location and different cruises cannot be directly inter-related (see Appendix IV for Level-2 MODIS chlorophyll and sea surface temperature data that support that variability).

5.3. Atmospheric correction

It is understood that the principle chosen to atmospherically correct the remote sensing images is biased towards the data collected in the field, as the remote sensing data was forced to fit in the range of the field measurements. An attempt to maintain the independence of the analysis was to select one point from each cruise to perform the correction exclusively, even though the number of available field measurements was already limited. To some extent, however, it is also possible that the technique adopted served to resolve the issue of different spatial resolutions observed by each sensor, by defining the expected range of values.

Part 1) Applying bio-optical model to obtain η and b_{bp} (λ_0)

The backscattering coefficients obtained from inverting the one-termed reflectance model varied considerably for each point analysed, which may be a result of different water masses being sampled in each location. The amplitude of values, however, is in agreement with the ones found in the literature for the same region (see Toole and Siegel, 2001). Values for the spectral slope of suspended matter (η) were generated based on the b_{bp} estimated, and for not just the five stations selected for atmospheric correction, but also for all the subsequent slope estimations, the values were higher and quite different from the ones available in the literature: a fixed value of 0.48 for the SBC, by Kostadinov et al (2007); and a fixed value of 1.0337 for global applications, by Maritorena et al (2002). The work of Kostadinov et al (2007) is an optimisation and regionalisation of the GSM01 Bio-Optical Model of Maritorena et al (2002). They used all data available in the PnB Project to generate the slope, which theoretically increased the chances of the final value to be representative of the area. However, the final output was a fixed value to represent all oceanographic situations in the SBC, which unfortunately is an inappropriate simplification, as the water properties in the region are highly variable. Moreover, it was documented that such optimisation did not result in improvements towards better representing the environment. An interesting aspect of this M.Sc. was that η were estimated for all individual points, rather than using a single global or local model-generated value. In contrast, only very limited wavelengths and points were available. For the purposes of this study, however, the slopes obtained met a minimum requirement, i.e. they were able to satisfactorily predict R_{rs} for the reference wavelengths as shown in Part 2). Regardless of which η and b_{bp} value seems more representative, it is accepted that little is known about the variability of those in Case-2 waters, so that many of the models uncertainties are linked to their probable variability in time and space (Siegel et al., 2005; Kostadinov et al., 2007; Whitmire et al., 2007; Zawada et al., 2007).

Part 2) Applying a reflectance model to estimate field R_{rs} for MODIS and MERIS' wavelengths

Another important consideration of the methodology proposed in this study is that it is almost entirely based on signals retrieved in a reference wavelength ~443 nm. As expected, therefore, relative errors of estimations are at their minimum at that wavelength. The high variability around 550 nm in the original field dataset might have reflected in the higher relative errors in the estimation of R_{rs} for wavelength 510 nm.

Regarding the final corrected spectra for MODIS and MERIS, the peaks at around 550 nm reflect the importance of particulate backscattering in the system. Likewise, the non-zero reflectance observed above 700 nm suggests that backscattering plays an important role in the red spectral region (Toole et al., 2000; Toole and Siegel, 2001), which also exemplifies why a classic atmospheric correction approach would not be suitable for these areas (Doxaran et al., 2006). Strong absorption around 440 nm followed by a sudden slope towards 550 nm observed for both MODIS and MERIS, for PnB-174 stations 7 and 6, can be related to a fertilisation episode, especially when those same stations present increased reflectances at 680 nm. These are believed to be a proxy for phytoplankton concentration, since solar-stimulated chlorophyll fluorescence are frequently observed over that part of the spectrum (Perry, 2003). What is interesting is that phytoplankton fluorescence varies according to nutrient availability and illumination conditions, which in practice intrigues the investigation of which environmental change might have occurred in the waters at those dates and locations. A possibility is that a combination of spring winds hitting the coast (as expected for that period of the year) with the light but persistent rain registered in the continent might have created ideal conditions for phytoplankton growing (Kudela et al., 2006). That is because nutrient availability and the maintenance of the organisms in the water column depend on the vertical stability of the system as a whole, which are made favourable when persistent but not extreme events hit a certain area (Perissinotto et al., 1990; Lalli and Parsons, 1997).

Because no in-situ chlorophyll *a* estimations were available for that date in particular in order to corroborate the signal observed, an estimation of the concentration was obtained by applying Equation 7 (Page 22). For both stations, chlorophyll *a* was estimated to be around 7 mg/m^3, which is a high amount if compared to the measured chlorophyll for other dates and stations in this study. Looking at the MODIS Level 2 products[5] for the date (Appendix IV), high and possibly overestimated values of chlorophyll *a* were observed (>70 mg/m^3), which is

[5] Chlorophyll *a*: For MODIS-Aqua, it is generated with the OC3 algorithm, a blue-to-green ratio that uses the largest of the $R_{rs}(443)/R_{rs}(551)$, and $R_{rs}(488)/R_{rs}(551)$ ratios (Morel et al, 2007). For SST, the MODIS' bands used in the algorithm are 20, 22, 23, 31 and 32, as explained in Brown, O. B. and Minnett, P. J. (1999). MODIS Infrared Sea Surface Temperature Algorithm Algorithm Theoretical Basis Document Version 2.0. 85 p.

likely to represent a failure in the algorithm utilised, a known artefact in complex Case-II waters (Ruddick et al., 2000). If the absolute values are ignored however, and attention is centred on the distribution and shape of the patches, classic oceanographic conditions of fertilisation are characterised, with accumulation/trapping of high *chl-a* concentrations around the shallower areas (islands), and dissipation towards the ocean. That is also highlighted by the SST map for the date, where colder waters penetrate the SBC where Points 7 and 6 are located. Colder waters, together with the chlorophyll estimations, provide evidence that cruise PnB-174 sampled highly productive waters, as indicated in the remote sensing signal.

The resulting spectra can be compared with the general shape and amplitude of values presented by Toole and Siegel (2001) for the SBC, especially between 450 nm and 600 nm, indicating that even though there were only a few available data points for this experiment, they are representative of the region as a whole. Realizing that also reassures the quality and confidence on the available data. That, together with the values obtained for the spectral slope of backscattering, could also suggest that waters with Case-I characteristics may have been observed and dominated some situations in this work. A similar conclusion was made by Kostadinov et al (2007).

Considering Figure 5 presented (Page 32), the fact that there is not a strong similarity in shape between the mean and standard deviation spectrum of each sensor indicates that the constituents that impact R_{rs} change independently of each other, which is expected for complex regions like the SBC (Toole and Siegel, 2001). As previously stated, the mean spectrum shape may differ between sensors due to the fact that they are collecting information in different wavelengths. Also, the continuous line joining all discrete wavelengths may create an illusion that the sensors are more different than in reality. In fact, the behaviour of the spectrum in between two wavelengths is unknown at this stage.

The double peak suggested by MERIS data at 490 and 560 nm can be associated with peaks of the same magnitude and shape in the work of Toole and Siegel (2001), who profiled the SBC waters with a hyperspectral instrument. Modelled values for the first wavelength of both sensors (412.5 nm) are of suspiciously high magnitudes, which may indicate that the atmospheric correction approach here considered underestimated the effect of aerosols, strong scatterers in that part of the spectrum (Ruddick et al., 2003; Ruddick et al., 2006; Sorensen et al., 2007). Also, in some cases, a drop in reflectance was noticed in the blue region, and that may be an indication of the absorption by CDOM (Ruddick et al., 2000). The large variability of values observed could also be related to uncertainties in the particulate absorption for the blue region of the spectrum collected in the field (Boss et al., 2007).

Minimal effort was put into correcting the points that failed the atmospheric correction procedure, as any unknown and unnecessary sources of uncertainty could have had compromised the analysis to a serious extent. So, to remain as confident on the results as possible, it was preferred to exclude those, even though a reduction in sampling points is known to jeopardise statistical analysis.

Looking back at the atmospheric correction options, it is possible that in the near future MERIS may be incorporated into the current MODIS processing package (SeaDAS), which has been widely tested and performs quite well in many applications. If so, remote sensing reflectances from both sensors would be derived using the same algorithms, sources and look-up tables. That would make it possible to use Level 2 products of both sensors (i.e. R_{rs}) directly in the merging, allowing to skip or simplify parts of the pre-processing and atmospheric correction procedure described in this study.

5.4. Expanding MODIS and MERIS spectra to all available points

The spectral slopes of suspended matter estimated for the atmospherically corrected points could be highly influenced by the number of discrete bands available during the calculations, as an average of the η for each available spectrum is used in the calculation.

If compared to the field data estimations, particle backscattering spectra for MODIS and MERIS resulted in more variable b_{bp} estimations, which could be related to surrounding water masses being considered in the averaging process.

The resulting R_{rs} for field data, MODIS and MERIS in the same 21 wavelengths replicate the main features depicted after atmospheric correction, providing some confidence on the methodology adopted. The absolute values were retrieved quite successfully for wavelengths 412.5 – 560 nm, as Table 8 indicates. The fluorescence peaks, however, are smoothed out in the majority of cases, which can be related to the choice of a^*_{ph}, the chlorophyll *a* specific absorption coefficient, even though the spectrum is believed to represent the most adequate one for the SBC (Kostadinov et al., 2007). It is accepted that significant changes in a^*_{ph} occur with changes in phytoplankton's distribution in time and space, cell size and pigment composition (Millán-Núñez et al., 2004). In highly productive waters like the SBC that possibility must be considered, especially when remembering that only a few sampling units were studied in this M.Sc., which may not correspond to the area as a whole, as studied by other authors.

In fact, the models used in this study consider chlorophyll *a* as the main pigment, which is a classic situation for Case-I waters, and might not necessarily represent coastal waters. Also, a more thorough understanding of the environment would depend on making possible the differentiation between different phytoplankton groups, i.e. microplankton, pikoplankton, nanoplankton, etc, as their presence/absence may infer different environmental conditions and ecosystem relationships (Siegel et al., 2005).

Toole and Siegel (2001) mention that the methods for estimating b_{bp} and R_{rs} for full spectra, as undertaken in this study, are clearly "not the best approach for spectral regions where non-linear scattering processes (i.e. Raman scattering and chlorophyll *a*, and CDOM fluorescence) are active". Those regions are located beyond 650 nm, and in many studies they are excluded for the analysis. Here, they were maintained to support the outcome of the research, which is ultimately to merge the spectra of MODIS and MERIS into a common spectrum, even though uncertainties are likely to dominate some regions. In fact, the relative errors in retrieving the original atmospherically corrected values after applying the forward model are large for wavelengths greater than 700 nm. From the graphs, it can be seen that the model tended to bring the near-infrared signal as close to zero as possible, as it would in clear Case-I waters, not depicting the backscattering influence which is potentially active in this region (and as observed in the atmospherically corrected spectra).

5.5. Spectral Merging

Merging MODIS and MERIS through multi-linear regression analysis represented some important theoretical issues. The first is that only eight calibration points were used to extract the regression coefficients, which is clearly not enough for a robust statistical analysis (Moore and McCabe, 1998). The second is that MODIS and MERIS' data may not have varied independently of each other, i.e. statistically they were considered “collinear” variables. To understand when that might have happened, it is important to first look at Table 9 (Page 36).

For some wavelengths, even though the overall p-value was low (smaller than the significance level of 0.05), all the individual coefficients’ p-values were high (not significant). That indicates that the data fitted the model well, even though none of the independent variables (MODIS and MERIS) had a statistically significant impact on predicting the dependent one (field observations) (Motulsky, 2002). That is possible when the independent variables are highly correlated and explain the same part of the variation in the dependent variable (i.e. they are collinear), so that the significance of their coefficients is divided up between them (Princeton University, 2007). That was the case for the first six bands of MODIS and MERIS.

In practice it could signify that, for those six wavelengths, MODIS and MERIS are extracting similar information from the ocean. It could also be directly related to the original range of wavelength represented by the field measurements, as the model might not have been successful in predicting the spectra behaviour beyond those wavelengths, as a result of its linearity assumptions (Toole and Siegel, 2001).

In other cases, however, neither the overall regression, nor the coefficients’ p-values were statistically significant. That was dealt with by shifting the analysis to a different kind of interpretation: that of practical importance. If the final results (i.e. applying the significant or non-significant coefficients to the seven validation points) improved the initial data (accuracy-wise), the technique was considered successful. The improvement was measured through the Root Mean Square Error between the estimated value and the value it should have been (from field data). Ultimately, even though the analysis was wavelength-based, the goal was to observe if merging the sensors improved the estimations throughout the spectrum as a whole.

Clearly, in 50% of the time only one sensor was statistically selected to estimate the “merged” value for that band, and that was a limitation while interpreting the final result. Still, for some important bands for the Ocean Colour community (443 and 490 nm, for example), both sensors contributed with the overall fit. There is a possibility that, had the study considered more sampling points, the regression would have included both sensors in the model, and the overall statistics would have been improved.

Important to note that not only β and α, but also the less than satisfactory R^2 and Adjusted R^2 results can also be directly related to the limited number of sampling units considered.

By analysing the results of the validation (Figures 8 and 9, page 38 and 39), it is possible to see that the accuracy of the estimations improved for all wavelengths, apart from 412.5 nm, which was probably a consequence of atmospheric correction failure in the blue, as previously explained. After removing the influence of that band, the difference between the RMSEs obtained from MODIS and MERIS separately and from the merged data is a good indication that the accuracy of the estimations are higher when the merged data is considered. Somehow, the merged dataset could and should have been statistically compared with the MODIS and MERIS spectra obtained after atmospheric correction, and not after the inverse and forward models, as those steps were needed to generate the merged spectra as well, which might have introduced some bias in the analysis. In Appendix V, however, it is possible to make a visual comparison among initial field data, atmospherically corrected remote sensing data and the merged output, as suggested.

Furthermore, the errors that are still evident in the merged spectra may be due to features that can't be explained by either one of the sensors. Regardless, it is interesting to observe how well the merging worked considering such limitations, which indicates that the technique could be improved in further studies.

To this moment, however, it is risky to state if the merged dataset explains the environment differently from MODIS or MERIS alone. It is apparent that the combination of the sensors' wavelengths resulted in a smoother spectra, as more discrete wavelengths are included. If MODIS was considered alone (and just the 9 initial bands), no features around the red-edge would be delineated. If MERIS was considered alone (13 bands), a rougher signal around the green part of the spectrum would be observed. That is, however, directly related to applying the bio-optical and reflectance models, and not to merging the data through regression. In order to know if the smoother spectra actually mean a gain in information, further investigations should be undertaken, such as using independent data to test the results (hyperspectral field measurements, for example), and applying the technique to a larger set of pixels, so the improvement could be better visualised. Here, the role of the inverse and forward reflectance models in standardising MODIS and MERIS data suggested the potential of the technique in improving the accuracy of the outputs.

5.6. Limitations and recommendations

Important to notice that errors were propagated throughout the entire analysis, and their relative importance was not evaluated in depth. Uncertainties during extrapolating below-water reflectance to above-water reflectance; during all steps of calibration and conversion; errors and bias in atmospheric correction; inherent errors with the reflectance and bio-optical models (as their assumptions and limitations were fully incorporated); simplifications due to not considering the spectral response function of each sensor in the analysis; bias in utilising field absorption measurements to model reflectances for both sensors and field; limitation in considering the field data as “absolute” and free of errors; and finally the uncertainties in retrieving the regression’s coefficients and equations, due in part to the limited number of sampling units. The latter, in fact, limited the capability to indicate how much each sensor actually contributed with the overall regression, information that, if reliable, could be quite valuable in assessing individual performances.

The methodology concentrated on points where field measurements were available only. Therefore, it was a theoretical approach, as no image was generated at this stage. A visualisation of the outputs in the form of images would be of great value in the future. As shown through the Level-2 data in Appendix IV, a lot of information on shape and distribution of the ocean colour in the area as a whole can be closely related to what is affecting the points of interest.

Disregarding the theoretical benefits of combining MODIS and MERIS datasets, a point that needs to be taken into account is the availability of MERIS and MODIS match-ups. While finding coincident images for the SBC region, it was observed that MODIS and MERIS would overpass the same area with a 1-2 days lag. In the future, it would be interesting to adapt the methodology here explained to account for the temporal variability of the oceanographic features, so that MODIS and MERIS from different dates could be merged together.

Another inherent limitation of the work is related to the field measurements. Those represent an infinitely small fraction of the surface waters if compared to the amount of information present or averaged within every pixel in a sensor. Proper sampling strategies could be planned, but the high costs involved in field experimentation are the usual limitations. Depending on the situation, the remotely sensed data can be under or overestimating the data collected in the field, but the difference in results does not mean that either is wrong. Rather, it indicates that they are referring to information in different scales. The issue is not as big a problem in clear open ocean as it is in Case-II waters, where many water masses with different properties interact within various spatial and temporal scales. Increasing the spatial resolution of sensors is an alternative to address such issues. MERIS Full Resolution images are a good example (300 m spatial resolution). Even though those were not used in this study (as they were not available for the place and period needed), it is believed that the methodology described in this M.Sc. could be reproduced for higher resolution data in the future, with expected improved results.

General recommendations follow:

- To apply the technique for more sampling units. Global datasets like the NOMAD could be used for such, even though they focus primarily on case 1 waters. In case of productive waters like the SBC, an alternative is to analyse the area per season, when the chance of sampling more homogeneous data is increased. Once the temporal variability is well characterised, conclusions regarding the whole area could be reached.
- To generate chlorophyll-*a* estimations from each sensor separately and from the merged spectra, to investigate if the merged product provides more accurate estimations of the concentrations;
- To perform spatial merging as the one of Pottier et al (2006) in order to make MODIS and MERIS' spatial resolutions comparable;
- To automate the methodology to avoid systematic errors and improve efficiency;
- To apply the techniques to all pixels in the image, in order to obtain visualisations of the merging through images;
- To experiment the methodology for MERIS Full Resolution images, improving spectral and spatial resolutions of final outputs (considering both spectral and spatial merging are performed);
- To consider the spectral response function of the sensors to help decide the importance of each sensor in describing each wavelength;
- To extract the uncertainties in each of the steps, and to incorporate them in the models;
- To consider different field sampling strategies. For example, to collect more data over scales comparable to the sensor's pixel sizes, so that the match-ups can be more representative;

6. Conclusions

Regarding the first Research Question:
Despite MODIS and MERIS' inherent differences in spectral and spatial resolution, design and orbit patterns, is it possible to perform a spectral merging of their remote sensing reflectance estimations?

The study showed that it was possible to perform spectral merging of MODIS and MERIS remote sensing reflectance data. Since common calibration and atmospheric correction procedures were adopted for both sensors, it is believed that the individual sensor's outputs were relatively comparable in terms of the magnitude of the values and in which information they were extracting from the same area.

Regarding the second Research Question and Research Hypothesis:
Does merging MODIS and MERIS remote sensing reflectances improve the accuracy of the final retrievals (in terms of how similar those results are from reflectances collected in the field)?

Merging MODIS and MERIS remote sensing reflectances improved the overall accuracy of the estimations, even though the results are biased towards the model utilised. When compared to the field measurements, the errors in the estimations with the merged spectra were 0.75 smaller than MODIS errors alone and nearly twice smaller than MERIS' estimated errors.

Regarding the third Research Question and Research Hypothesis:
Considering that more discrete wavelengths will determine the merged spectrum, will more oceanographic features actually be depicted?

Smoother spectra were generated taking into consideration all the available wavelengths of MODIS and MERIS. However, it was not possible to clearly relate the increase in the number of discrete wavelengths per spectrum to better depiction of oceanographic features. In the future, the visualisation of the results under the form of images could possibly provide such information.

7. Bibliography

Antoine, D. and Morel, A. (1999). A multiple scattering algorithm for atmospheric correction of remotely sensed ocean colour (MERIS instrument): principle and implementation for atmospheres carrying various aerosols including absorbing ones. *International Journal of Remote Sensing* 20, 1875-1916.

Antoine, D. and Morel, A. (2005). Atmospheric Correction of the MERIS observations Over Ocean Case 1 waters. Villefranche sur Mer, Laboratoire D'Oceanographie de Villefranche.

Antoine, D. F., D'ortenzio, S. B., Hooker, G., Bécu, B., Gentili, D. and Scott, A. (2008). Assessment of uncertainty in the ocean reflectance determined by three satellite ocean color sensors (MERIS, SeaWiFS, MODIS) at an offshore site in the Mediterranean Sea (BOUSSOLE project). *Journal of Geophysical Research* 113.

Antoine, D. M., Chami, H., Claustre, F., D'ortenzio, A., Morel, G., Bécu, B., Gentili, F., Louis, J., Ras, E., Roussier, A. J., Scott, D., Tailliez, S. B., Hooker, P., Guevel, J., Desté, F., Dempsey, C. and Adams, D. (2006). BOUSSOLE: a joint CNRS-INSU, ESA, CNES and NASA Ocean Color Calibration And Validation Activity. NASA Technical memorandum N° 2006-214147, NASA/GSFC. Greenbelt, MD, 61 p.

Atkinson, L. P., Brink, K. H., Davis, R. E., Jones, B. H., Paluszkiewicz, T. and Stuart, D. W. (1986). Mesoscale Hydrographie Variability in the Vicinity of Points Conception and Arguello During April-May 1983: The OPUS 1983 Experiment. *J. Geophys. Res.* 91.

Austin, R. W. (1974). The remote sensing of spectral radiance from below the ocean surface. Optical Aspects of Oceanography. N. G. J. a. E. S. Nielson**:** 317-344.

Babin, M. and Stramski, D. (2002). Light absorption by particles in the near infrared spectral region. *Limnol. Oceanogr.* 47, 911-915.

Bailey, S. W., Hooker, S. B., Antoine, D., Franz, B. A. and Werdell, P. J. (2008). Sources and assumptions for the vicarious calibration of ocean color satellite observations. *Appl. Opt.* 47, 2035-2045.

Bailey, S. W. and Werdell, P. J. (2006). A multi-sensor approach for the on-orbit validation of ocean color satellite data products. *Remote Sensing of Environment* 102, 1-2, 12-23.

Bissett, W. P., Arnone, R., Debra, S., Dieterle, D. A., Dye, D., Kirkpatrick, G. J., Schofield, O. M. and Vargo, G. A. (2005). Predicting the optical properties of the West Florida Shelf: resolving the potential impacts of a terrestrial boundary condition on the distribution of colored dissolved and particulate matter. *Marine Chemistry* 95, 3-4, 199-233.

Blondeau-Patissier, D. (2004). Comparison of bio-physical marine products from SeaWiFS, MODIS and a bio-optical model with in situ measurements from Northern European waters. *Journal of Optics A: Pure and Applied Optics* 6, 875-889.

Boss, E., Collier, R., Larson, G., Fennel, K. and Pegau, W. (2007). Measurements of spectral optical properties and their relation to biogeochemical variables and processes in Crater Lake, Crater Lake National Park, OR. *Hydrobiologia* 574, 1, 149-159.

Bourg, L., D'alba, L. and Colagrande, P. (2008). Technical Note - MERIS Smile Effect characterisation and correction. 2.

Bray, N. A., Keyes, A. and Morawitz, W. M. L. (1999). The California Current system in the Southern California Bight and the Santa Barbara Channel. *J. Geophys. Res.* 104.

Bricaud, A., Morel, A. and Prieur, L. (1981). Absorption by dissolved organic matter of the sea (yellow substance) in the UV and visible domains. *Limnol. Oceanogr.* 26, 1, 43-53.

Brown, O. B. and Minnett, P. J. (1999). MODIS Infrared Sea Surface Temperature Algorithm Algorithm Theoretical Basis Document Version 2.0. 85 p.

Campbell, J. W. (1996). Development of Algorithms and Strategies for Monitoring Chlorophyll and Primary Productivity in Coastal Ocean, Estuarine and Inland Water Ecosystems. Quarterly Technical Report.

Cannizzaro, J. P. and Carder, K. L. (2006). Estimating chlorophyll a concentrations from remote-sensing reflectance in optically shallow waters. *Remote Sensing of Environment* 101, 1, 13-24.

Ciotti, A. M. and Bricaud, A. (2006). Retrievals of a size parameter for phytoplankton and spectral light absorption by colored detrital matter from water-leaving radiances at SeaWiFS channels in a continental shelf region off Brazil. *Limnol. Oceanogr.: Methods* 4, 237–253.

Dall'olmo, G., Gitelson, A. A., Rundquist, D. C., Leavitt, B., Barrow, T. and Holz, J. C. (2005). Assessing the potential of SeaWiFS and MODIS for estimating chlorophyll concentration in turbid productive waters using red and near-infrared bands. *Remote Sensing of Environment* 96, 2, 176-187.

Doxaran, D., Babin, M. and Leymarie, E. (2007). Near-infrared light scattering by particles in coastal waters. *Optics Express* 15, 20, 12834-12849.

Doxaran, D., Cherukuru, N. and Lavender, S. J. (2006). Apparent and inherent optical properties of turbid estuarine waters: measurements, empirical quantification relationships, and modeling. *Applied Optics* 45, 10, 2310-2324.

ESA (2005). GlobColour Project. Available at http://www.globcolour.info/project_objectives.html.

ESA (2006). MERIS Product Handbook. European Space Agency. Available at http://envisat.esa.int/handbooks/meris/.

Fargion, G. S., Mcclain, C. R., Franz, B. A., Wilding, J. G. and Gales, J. M. (2003). Operational Merging of MODIS and seaWiFS Ocean Color Products at Level-3. MODIS Validation, Data Merger and Other Activit ies Accomplished by SIMBIOS Project: 2002-2003.

Feldman, G. C. and Mcclain, C. R. (2007a). OceanColor Forum, Ocean Color Web. Eds. Kuring, N., Bailey, S. W., Thomas, D., Franz, B. F., Meister, G., Werdell, P. J., Eplee, R. E., MacDonald, M., Rubens, M.NASA Goddard Space Flight Center. Accessed in Nov. 2007. Available at http://oceancolor.gsfc.nasa.gov/forum/oceancolor/topic_show.pl?pid=10530;hl=convert%20reflectance#pid10530.

Feldman, G. C. and Mcclain, C. R. (2007b). OceanColor Forum, Ocean Color Web. Eds. Kuring, N., Bailey, S. W., Thomas, D., Franz, B. F., Meister, G., Werdell, P. J., Eplee, R. E., MacDonald, M., Rubens, M.NASA Goddard Space Flight Center. Accessed in Nov. 2007. Available at http://oceancolor.gsfc.nasa.gov/forum/oceancolor/topic_show.pl?pid=10290;hl=convert%20reflectance#pid10290.

Fournier-Sicre, V. and Belanger, S. (2002). Intercomparison of SeaWiFS and MERIS marine products on Case 1 waters. Proc. of Envisat Validation Workshop, Frascati, Italy.

Gilerson, A., Zhou, J., Hlaing, S., Ioannou, I., Gross, B., Moshary, F. and Ahmed, S. (2008). Fluorescence component in the reflectance spectra from coastal waters. II. Performance of retrieval algorithms. *Optics Express* 16, 4, 2446 - 2460.

Gordon, H. R., Brown, O. B., Evans, R. H., Brown, J. W., Smith, R. C., Baker, K. S. and Clark, D. K. (1988). A Semianalytic Radiance Model of Ocean Color. *J. Geophys. Res.* 93, D9, 10,909 - 910,924.

Gordon, H. R., Brown, O. B. and Jacobs, M. M. (1975). Computed Relationships Between the Inherent and Apparent Optical Properties of a Flat Homogeneous Ocean. *Appl. Opt.* 14, 2, 417-427.

Gregg, W. W., Esaias, W. E., Feldman, G. C., Frouin, R., Hooker, S. B., Mcclain, C. R. and Woodward, R. H. (1998). Coverage opportunities for global ocean color in a multimission era. *Geoscience and Remote Sensing, IEEE Transactions on* 36, 5, 1620-1627.

GSFC/NASA (2007). MODIS Web. Available at http://modis.gsfc.nasa.gov/.

Harms, S. and Winant, C. D. (1998). Characteristic patterns of the circulation in the Santa Barbara Channel. *J. Geophys. Res.* 103.

Heap, A., Bryce, S., Ryan, D., Radke, L., Smith, C., Smith, R., Harris, P. and Heggie, D. (2001). Australian Estuaries & Coastal Waterways: A geoscience perspective for improved and integrated resource management. Australian Geological Survey Organisation, Record 2001/07. Available at http://dbforms.ga.gov.au/pls/www/npm.ozest.show_mm?pBlobno=12885.

Hu, C., Carder, K. L. and Muller-Karger, F. E. (2000). Atmospheric Correction of SeaWiFS Imagery over Turbid Coastal Waters: A Practical Method. *Remote Sensing of Environment* 74, 2, 195-206.

Hu, C., Wang, Y., Yang, Q., He, S., Hu, L. and He, M. (2007). Comparison of Ocean Colour Data Products from MERIS, MODIS, and SeaWIFS: Preliminary results for the East China Seas. Envisat Symposium 2007, Montreux, Switzerland 23–27 April 2007.

IOCCG (2000). Remote Sensing of Ocean Colour in Coastal, and Other Optically-Complex, Waters. Sathyendranath, S. (ed.), Reports of the International Ocean-Colour Coordinating Group, No. 3, IOCCG, Dartmouth, Canada.

IOCCG (2007). Ocean-Colour Data Merging, Gregg, W. (ed.). Reports of the International Ocean-Colour Coordinating Group, no. 6, IOCCG, Dartmouth, Canada.

Jerlov, N. G. (1976). Marine Optics, Elsevier Oceanography Series, 5. 199 p.
Kostadinov, T. S., Siegel, D. A., Maritorena, S. and Guillocheau, N. (2007). Ocean color observations and modeling for an optically complex site: Santa Barbara Channel, California, USA. *Journal of Geophysical Research* 112, 15.
Kudela, R. M., Garfield, N. and Bruland, K. W. (2006). Bio-optical signatures and biogeochemistry from intense upwelling and relaxation in coastal California. *Deep Sea Research Part II: Topical Studies in Oceanography* 53, 25-26, 2999-3022.
Kwiatkowska, E. J. and Fargion, G. S. (2002). Merger of ocean color information from multiple satellite missions under the NASA SIMBIOS Project Office. *Proceedings of the Fifth International Conference on Information Fusion* 1, 1, 291 - 298.
Lalli, C. M. and Parsons, T. R. (1997). Biological Oceanography an Introduction. The Open University 2nd Edition. Vancouver, Canada**:** 39-73.
Lee, Z. P., Carder, K. L., Steward, R. G., Peacock, T. G., Davis, C. O. and Mueller, J. L. (1997). Remote-sensing reflectance and inherent optical properties of oceanic waters derived from above-water measurements. *Proceedings of SPIE, the International Society for Optical Engineering* 2963, 160-166
Li, Y. (2003). Atmospheric Correction of SeaWiFS Imagery for Turbid Coastal and Inland Waters: Comment. *Appl. Opt.* 42, 6, 893-895.
Loisel, H. and Stramski, D. (2000). Estimation of the Inherent Optical Properties of Natural Waters from the Irradiance Attenuation Coefficient and Reflectance in the Presence of Raman Scattering. *Appl. Opt.* 39, 18, 3001-3011.
Longley, P. A., Goodchild, M. F., Maguire, D. J. and Rhind, D. W. (2007). Geographic Information Systems and Science. , 2nd Edition. John Wiley & Sons, Ltd. 517 p.
Maritorena, S., Morel, A. and Gentili, B. (1994). Diffise reflectance of oceanic shallow waters: Influence of water depth and bottom albedo. *Limnol. Oceanogr.* 39, 7, 1689-1703.
Maritorena, S. and Siegel, D. A. (2005). Consistent merging of satellite ocean color data sets using a bio-optical model. *Remote Sensing of Environment* 94, 4, 429-440.
Maritorena, S., Siegel, D. A. and Peterson, A. R. (2002). Optimization of a semianalytical ocean color model for global-scale applications. *Appl. Opt.* 41, 15, 2705-2714.
Mcclain, C. R., Esaias, W., Feldman, G., Frouin, R., Gregg, W. and Hooker, S. (2002). The Proposal for the NASA sensor intercalibration and merger for biological and interdisciplinary oceanic studies (SIMBIOS) Program, NASA/ GSFC., 54 p.
Mélin, F., Zibordi, G. and Djavidnia, S. (2007). Development and validation of a technique for merging satellite derived aerosol optical depth from SeaWiFS and MODIS. *Remote Sensing of Environment* 108, 4, 436-450.

Mélin, F., Zibordi, G. and Djavidnia, S. (2008). Merged series of normalized water leaving radiances obtained from multiple satellite missions for the Mediterranean Sea. *Advances in Space Research* In Press, Corrected Proof.

Mertes, L. A. K., Hickman, M., Waltenberger, B., Bortman, A. L., Inlander, E., Mckenzie, C. and Dvorsky, J. (1998). Synoptic views of sediment plumes and coastal geography of the Santa Barbara Channel, California. *Hydrological Processes* 12, 6, 967-979.

Millán-Núñez, E., Sieracki, M. E., Millán-Núñez, R., Lara-Lara, J. R., Gaxiola-Castro, G. and Trees, C. C. (2004). Specific absorption coefficient and phytoplankton biomass in the southern region of the California Current. *Deep Sea Research Part II: Topical Studies in Oceanography* 51, 6-9, 817-826.

Mobley, C. D. (1994). Light and Water, Academic Press. San Diego, California.

Moore, D. S. and Mccabe, G. P. (1998). Introduction to the practice of statistics, W.H. Freeman and Company 3rd Edition.

Morel, A. (1974). Optical properties of pure water and pure sea water, in. Optical Aspects of Oceanography. Edited by N.G. Jerlov and E.S. Nielsen. San Diego, California, Academic**:** 1-24.

Morel, A., Huot, Y., Gentili, B., Werdell, P. J., Hooker, S. B. and Franz, B. A. (2007). Examining the consistency of products derived from various ocean color sensors in open ocean (Case 1) waters in the perspective of a multi-sensor approach. *Remote Sensing of Environment* 111, 1, 69-88.

Morel, A. and Mueller, J. L. (2003). Standardizing the Extraterrestrial Solar Flux Spectrum. 17th CEOS Plenary, Colorado Springs, USA http://www.ioccg.org/groups/mueller.html.

Morel, A. and Prieur, L. (1977). Analysis of variations in ocean color. *Limnol. Oceanogr.* 22, 4, 709-722.

Mueller, J., Mcclain, C., Caffrey, B. and Feldman, G. (1998). The NASA SIMBIOS Program. *Backscatter. Accessed in August 2008. Available at* http://www.ioccg.org/reports/simbios/simbios.html.

Mueller, J. L., Fargion, G. S. and Mcclain, C. R. (2003a). Inherent Optical Properties: Instruments, Characterizations, Field Measurements and Data Analysis Protocols. Ocean Optics Protocols for Satellite Ocean Color Sensor Validation, Revision 4, Volume IV. Greenbelt, Maryland, NASA Goddard Space Flight Center. NASA/TM-2003-211621/Rev4-Vol.IV: 83.

Mueller, J. L., Fargion, G. S. and Mcclain, C. R. (2003b). Radiometric Measurements and Data Analysis Protocols. Ocean Optics Protocols for Satellite Ocean Color Sensor Validation, Revision 4, Volume III. Greenbelt, Maryland, NASA Goddard Space Flight Center. NASA/TM-2003-21621/Rev-Vol III: 84.

Ocean Explorers (2007). Exploring the Ocean with GIS: Physical Data – Bathymetry. Accessed in Dec. 2008. Available at http://www.exploreoceans.org/index.php?option=com_content&task=category&sectionid=5&id=15&Itemid=33

Otero, M. P. and Siegel, D. A. (2004). Spatial and temporal characteristics of sediment plumes and phytoplankton blooms in the Santa Barbara Channel. *Deep-Sea Research II* 51, 1129–1149.

Peijuan, W., Suhong, L., Xiang, Z., Yonghua, Q., Qijiang, Z. and Yanjuan, Y. (2003). The study on the method of monitoring and analyzing mineral environment with remote sensing images. Geoscience and Remote Sensing Symposium, 2003. IGARSS '03. Proceedings. 2003 IEEE International.

Perissinotto, R., Rae, C. M. D., Boden, B. P. and Allanson, B. R. (1990). Vertical stability as a controlling factor of the marine phytoplankton production at the Prince Edward Archipelago (Southern Ocean). *Marine Ecology Progress Series* 60, 205-209.

Perry, M. J. (2003). Optical Sensors. ALPS Workshop on Autonomous and Langrangian Platforms and Sensors. La Jolla, California, USA.

Pope, R. M. and Fry, E. S. (1997). Absorption spectrum (380-700 nm) of pure water. 2. Integrating cavity measurements. *Appl. Opt.* 36, 8710–8723.

Pottier, C., Garcon, V., Larnicol, G., Sudre, J., Schaeffer, P. and Le Traon, P. Y. (2006). Merging SeaWiFS and MODIS/Aqua Ocean Color Data in North and Equatorial Atlantic Using Weighted Averaging and Objective Analysis. *Geoscience and Remote Sensing, IEEE Transactions on* 44, 11, 3436-3451.

Preisendorfer, R. W. (1960). Recommendation on the standardization of concepts, terminology and notation of hydrologic optics. Scripps Inst. Of Oceanogr.**:** 96.

Princeton-University. (2008). "Data and Statistical Services (DSS). Interpreting Regression Output. ." Accessed in Jan.2008. Available at http://dss.princeton.edu/online_help/analysis/interpreting_regression.htm.

Robinson, I. S. (1985). Satellite Oceanography: An Introduction for Oceanographers and Remote-sensing Scientists. Chichester, England, Ellis Horwood Limited.

Ruddick, K., Park, Y. and Nechad, B. (2003). MERIS imagery of Belgian coastal waters: mapping of suspended particulate matter and chlorophyll-a. Proceedings of the MERIS Users workshop held in Frascati, 10-13 November 2003, ESA Special Publication SP-549.

Ruddick, K. G., Cauwer, V. D. and Parkd, Y.-J. (2006). Seaborne measurements of near infrared water-leaving reflectance: The similarity spectrum for turbid waters. *Limnol. Oceanogr.* 51, 2, 1167–1179.

Ruddick, K. G., Ovidio, F. and Rijkeboer, M. (2000). Atmospheric Correction of SeaWiFS Imagery for Turbid Coastal and Inland Waters. *Appl. Opt.* 39, 6, 897-912.

Samain, O., Geiger, B. and Roujean, J.-L. (2006). Spectral Normalization and Fusion of Optical Sensors for the Retrieval of BRDF and Albedo: Application to VEGETATION, MODIS, and MERIS Data Sets. *IEEE Transections on Geoscience and Remote Sensing* 44, 11, 3166-3179.

Siegel, D. A., Maritorena, S., Nelson, N. B. and Behrenfeld, M. J. (2005). Independence and interdependencies among global ocean color properties:

Reassessing the bio-optical assumption. *Journal of Geophysical Research* 110, 14.

Smith, R. C. and Baker, K. S. (1978). The bio-optical state of ocean waters and remote sensing. *Limnol. Oceanogr.* 23, 247-259.

Sorensen , K., Aas, E. and Hokedal, J. (2007). Validation of MERIS water products and bio-optical relationships in the Skagerrak. *International Journal of Remote Sensing* 28, 3, 555 - 568.

State of California (2007). Department of Water Resources - Data Exchange Center. Accessed in January 2009. Available at http://cdec.water.ca.gov/misc/DailyPrecip.html.

Strickland, J. D. H. and Parsons, T. R. (1972). A practical handbook of sea-water analysis, J. Fish. Res. Bd. Canada.

Thuillier, G., Herse, M., Simon, P. C., Labs, D., Mandel, H., Gillotay, D. and Foujols, T. (2003). The solar spectral irradiance from 200 to 2400 nm as measured by the SOLSPEC spectrometer from the ATLAS 1-2-3 and EURECA missions. *Sol. Phys.* 214, 1-22.

Toller, G. N., Isaacman, A., Kuyper, J. and Salomonson, V. (2006). MODIS Level 1B Product User's Guide. 57 p.

Toole, D. A. and Siegel, D. A. (2001). Modes and mechanisms of ocean color variability in the Santa Barbara Channel. *J. Geophys. Res.* 106.

Toole, D. A., Siegel, D. A., Menzies, D. W., Neumann, M. J. and Smith, R. C. (2000). Remote-Sensing Reflectance Determinations in the Coastal Ocean Environment: Impact of Instrumental Characteristics and Environmental Variability. *Appl. Opt.* 39, 3, 456-469.

Trishchenko, A. P., Hwang, B. and Li, Z. (2002). Atmospheric Correction of Satellite Signal in Solar Domain: Impact of Improved Molecular Spectroscopy. Twelfth ARM Science Team Meeting Proceedings, April 8-12, 2002, St. Petersburg, Florida.

Turner, A. and Millward, G. E. (2002). Suspended particles: Their role in estuarine biogeochemical cycles. *Estuarine, Coastal and Shelf Science* 55, 857-883.

Twardowski, M. S., Boss, E., Sullivan, J. M. and Donaghay, P. L. (2004). Modeling the spectral shape of absorption by chromophoric dissolved organic matter. *Marine Chemistry* 89, 1-4, 69-88.

Tzortziou, M., Herman, J. R., Gallegos, C. L., Neale, P. J., Subramaniam, A., Harding, J. L. W. and Ahmad, Z. (2006). Bio-optics of the Chesapeake Bay from measurements and radiative transfer closure. *Estuarine, Coastal and Shelf Science* 68, 1-2, 348-362.

Tzortziou, M., Subramaniam, A., Herman, J. R., Gallegos, C. L., Neale, P. J. and Harding, J. L. W. (2007). Remote sensing reflectance and inherent optical properties in the mid Chesapeake Bay. *Estuarine, Coastal and Shelf Science* 72, 1-2, 16-32.

Vermote, E. F., Tanre, D., Deuze, J. L., Herman, M. and Morcrette, J.-J. (1997). Second Simulation of the Satellite Signal in the Solar Spectrum, 6s: An Overview. *IEEE Transections on Geoscience and Remote Sensing* 35, 3, 675-686.

Wang, M. and Shi, W. (2007). The NIR-SWIR combined atmospheric correction approach for MODIS ocean color data processing. *Optics Express* 15, 24, 15722 - 15733.

Webster, I. T., Ford, P. W., Robson, B., Margvelashvili, N. and Parslow, J. S. (2003). Conceptual Models of the Hydrodynamics, Fine-Sediment Dynamics, Biogeochemistry, and Primary Production in the Fitzroy Estuary. Cooperative Research Centre for Coastal Zone, Estuary & Waterway Management Technical Report no.8.

Wen, X. (2008). A new prompt algorithm for removing the bowtie effect of MODIS L1B data. The International Archives of the Photogrammetry, Remote Sensing and Spatial Information Sciences Vol. XXXVII. Part B3b. Beinjing. Available at http://www.isprs.org/congresses/beijing2008/proceedings/3b_pdf/02.pdf.

Werdell, P. J. and Bailey, S. W. (2005). An improved in-situ bio-optical data set for ocean color algorithm development and satellite data product validation. *Remote Sensing of Environment* 98, 1, 122-140.

Whitmire, A. L., Boss, E., Cowles, T. J. and Pegau, W. S. (2007). Spectral variability of the particulate backscattering ratio. *Optics Express* 15, 11, 7019-7031.

Yang, X., Gu, X., Chen, L. and Zhang, H. (2007). Atmospheric correction of directional polarized ocean color sensors. Geoscience and Remote Sensing Symposium, 2007. IGARSS 2007. IEEE International.

Zawada, D. G., Hu, C., Clayton, T., Chen, Z., Brock, J. C. and Muller-Karger, F. E. (2007). Remote sensing of particle backscattering in Chesapeake Bay: A 6-year SeaWiFS retrospective view. *Estuarine, Coastal and Shelf Science* 73, 3-4, 792-806.

Zhang, C. C., Hu, S., Shang, F. E., Muller-Karger, Y., Li, M., Dai, B., Huang, X. and Hong, H. (2006). Bridging between SeaWiFS and MODIS for continuity of chlorophyll-a assessments off Southeastern China. *Remote Sensing of Environment* 102, 250-263.

Appendix I

Landsat 5 – TM
From U.S.G.S
(as shown in study area)

Bathymetry vector data from Ocean Explorers (2007). Available at http://www.exploreoceans.org/index.phpwse.pl

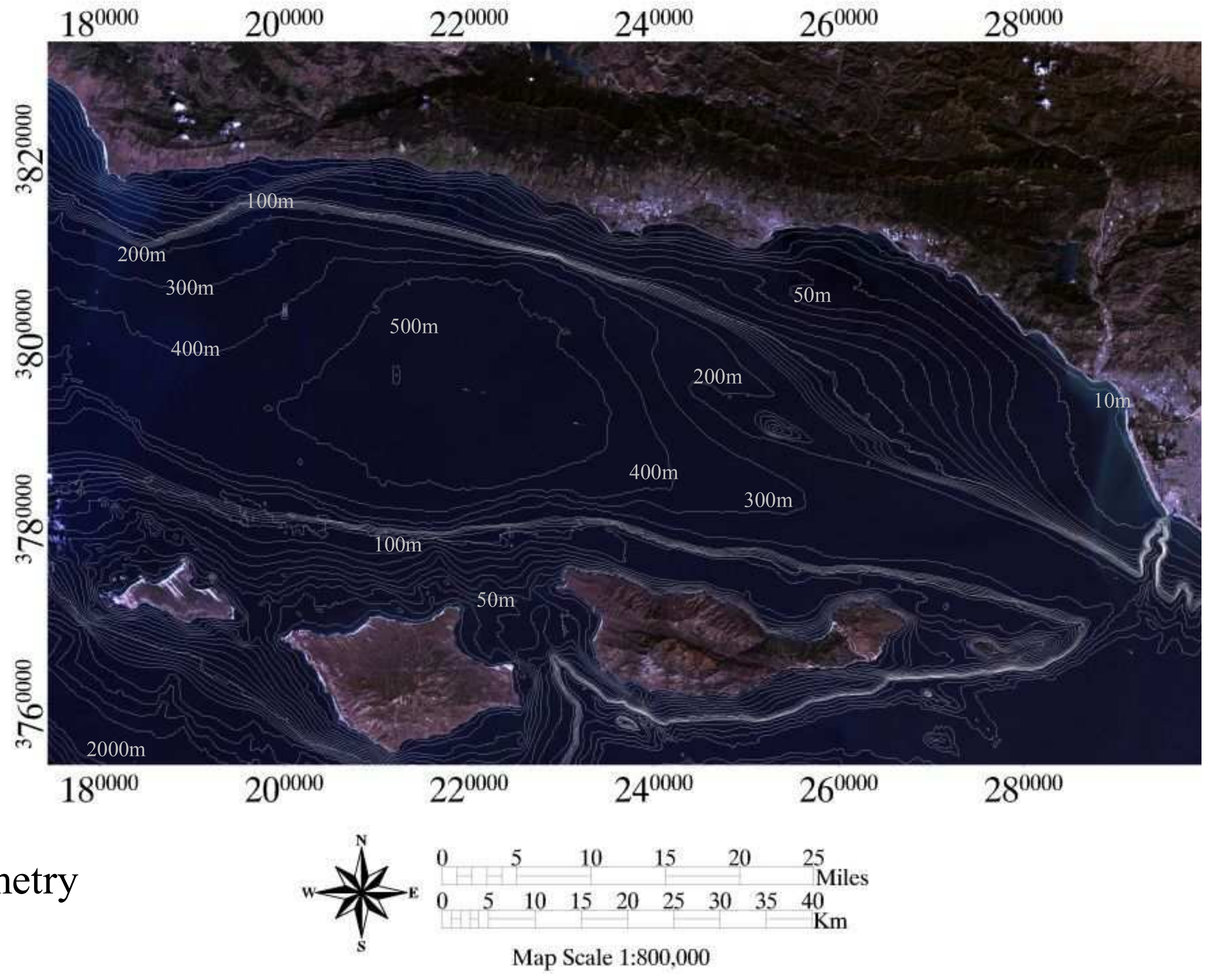

- Bathymetry

Appendix II

- Pre-processing

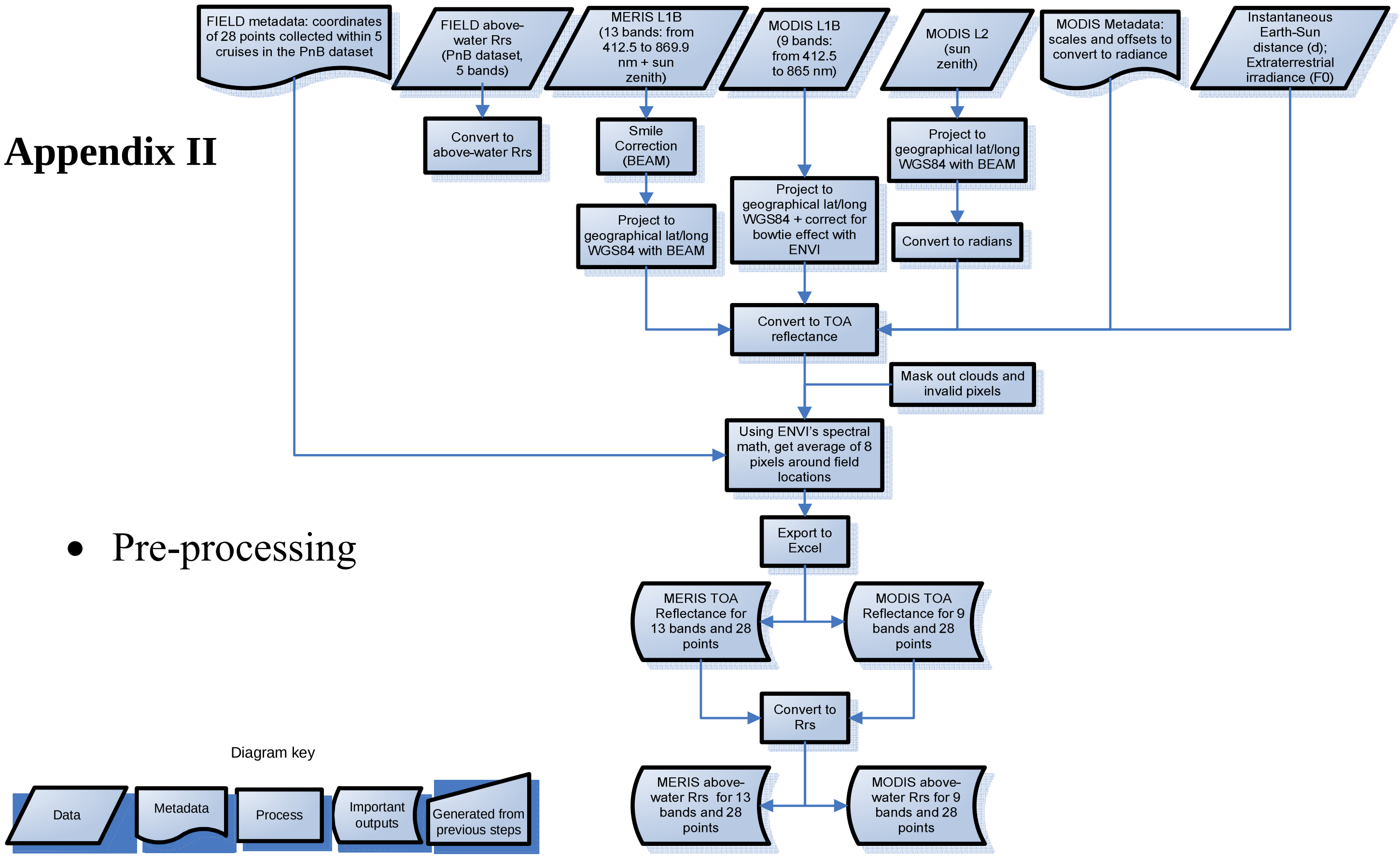

- Atmospheric correction

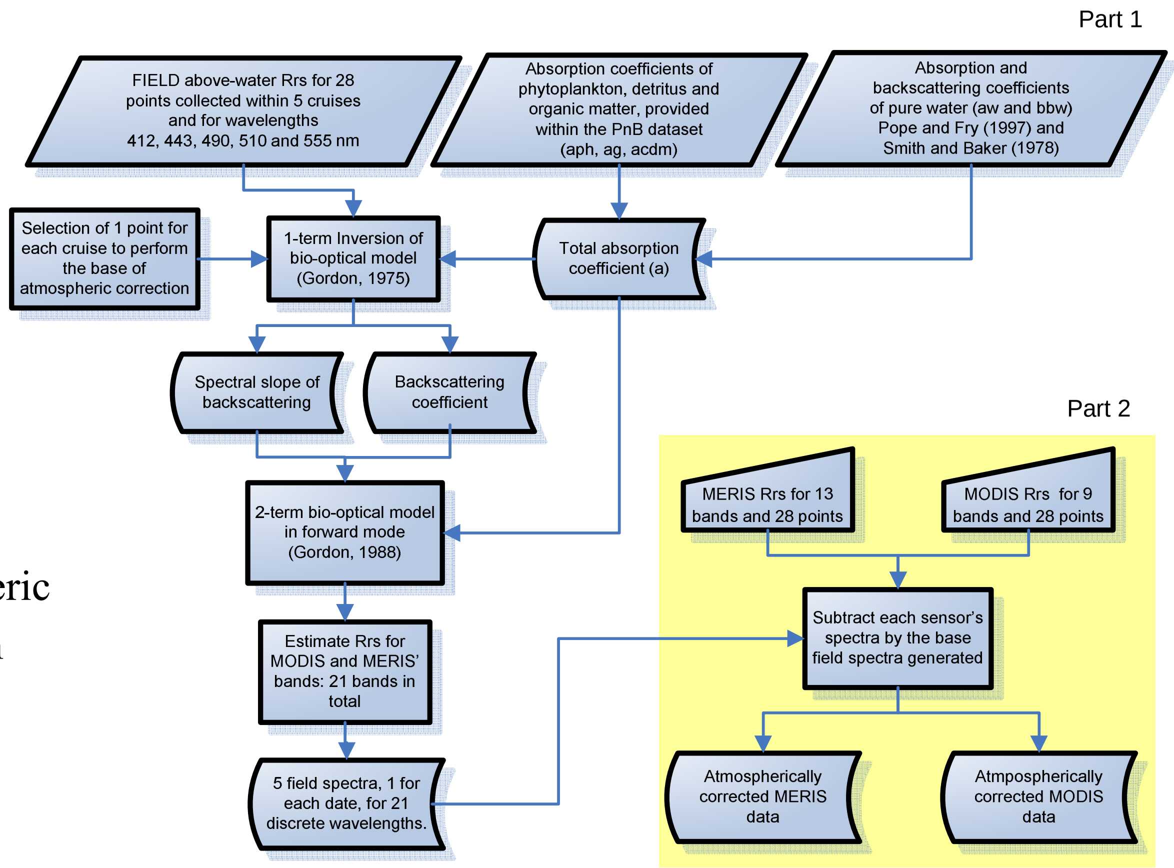

- Merging

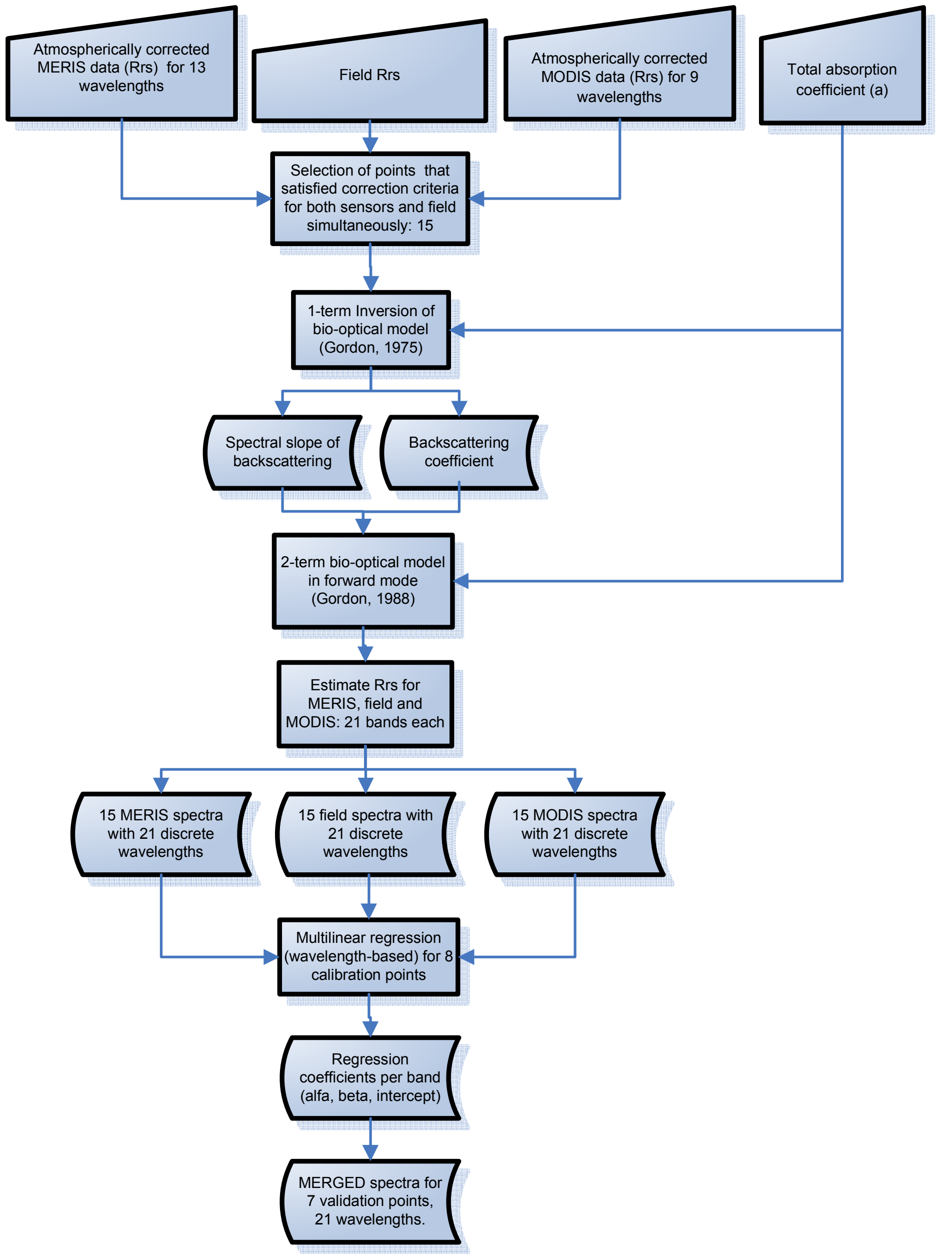

Atmospherically corrected MERIS data (Rrs) for 13 wavelengths
Field Rrs
Atmospherically corrected MODIS data (Rrs) for 9 wavelengths
Total absorption coefficient (a)
Selection of points that satisfied correction criteria for both sensors and field simultaneously: 15
1-term Inversion of bio-optical model (Gordon, 1975)
Spectral slope of backscattering
Backscattering coefficient
2-term bio-optical model in forward mode (Gordon, 1988)
Estimate Rrs for MERIS, field and MODIS: 21 bands each
15 MERIS spectra with 21 discrete wavelengths
15 field spectra with 21 discrete wavelengths
15 MODIS spectra with 21 discrete wavelengths
Multilinear regression (wavelength-based) for 8 calibration points
Regression coefficients per band (alfa, beta, intercept)
MERGED spectra for 7 validation points, 21 wavelengths.

Appendix III

- Definitions

Fluorescence

Phytoplankton and CDOM's ability to re-emit light in wavebands other than the absorbed light. Chlorophyll a is the primary fluorescence pigment, with a maximum emission at around 680 nm. The process is triggered according to environmental conditions, such as nutrient limitation and illumination conditions. It is also an IOP, but not as widely used in radiative transfer equations due to its current unpredictability.

Normalised water-leaving radiance

Derived from the calibrated top-of-atmosphere radiance measured by the satellite by removing the contribution of the atmosphere. It is normalised because it is corrected for BRDF (viewing angles dependence and effects of seawater anisotropy) (Pottier et al., 2006).

IOPs and AOPs

Originated with Preisendorfer (1960), IOPs "are quantities characterizing how a light field propagating through a given point in the medium is modified by the physical processes of absorption and scattering. The IOPs are material properties of the medium, and they are independent of the geometric properties of the vector light field. In contrast to the IOP, measurements of spectral irradiance and radiance propagating through a medium are dependent on the geometric distribution of the light field, as well as on the IOP of the medium. Under varying illumination conditions, such as variations in solar azimuth and zenith angle, these AOPs also vary" (Mueller et al, 2003).

Radiance

The radiant flux per unit solid angle from direction (θ, φ), per unit area, normal to the direction of flow (Mobley, 1994).

Remote sensing reflectance

R_{rs} is the "ratio of the water-leaving radiance to the downwelling irradiance just above the surface (Lee et al., 1997) . It is considered an apparent optical property, as it can be modified by the zenith-angular structure of the incident light field

(Preisendorfer, 1976; IOCCG Report 2000), and it can be directly related to the water constituents. R_{rs} is closely related to the surface reflectance (R) – the one derived from the atmospheric corrections – but makes use of upwelling radiance rather than irradiance IOCCG (2000).

Spectral Irradiance

The radiant flux per unit area through a point from all directions in the hemisphere above the surface. It is divided into "downward irradiance" and "upward irradiance". (Mobley, 1994).

Surface albedo

Determines in large part the amount of energy available to drive turbulent fluxes of heat and moisture. It is a crucial path to understand feedback mechanisms between radiance balance and its influence on climate and vegetation dynamics. In practice, it is defined as the upwelling irradiance divided by the downwelling irradiance (from Gao et al 2006, Analysis of temporal variations of surface albedo from MODIS, Proc. of SPIE Vol. 6298).

MODIS L2 chl-a and SST data downloaded from
http://oceancolor.gsfc.nasa.gov/cgi/browse.pl

Appendix IV

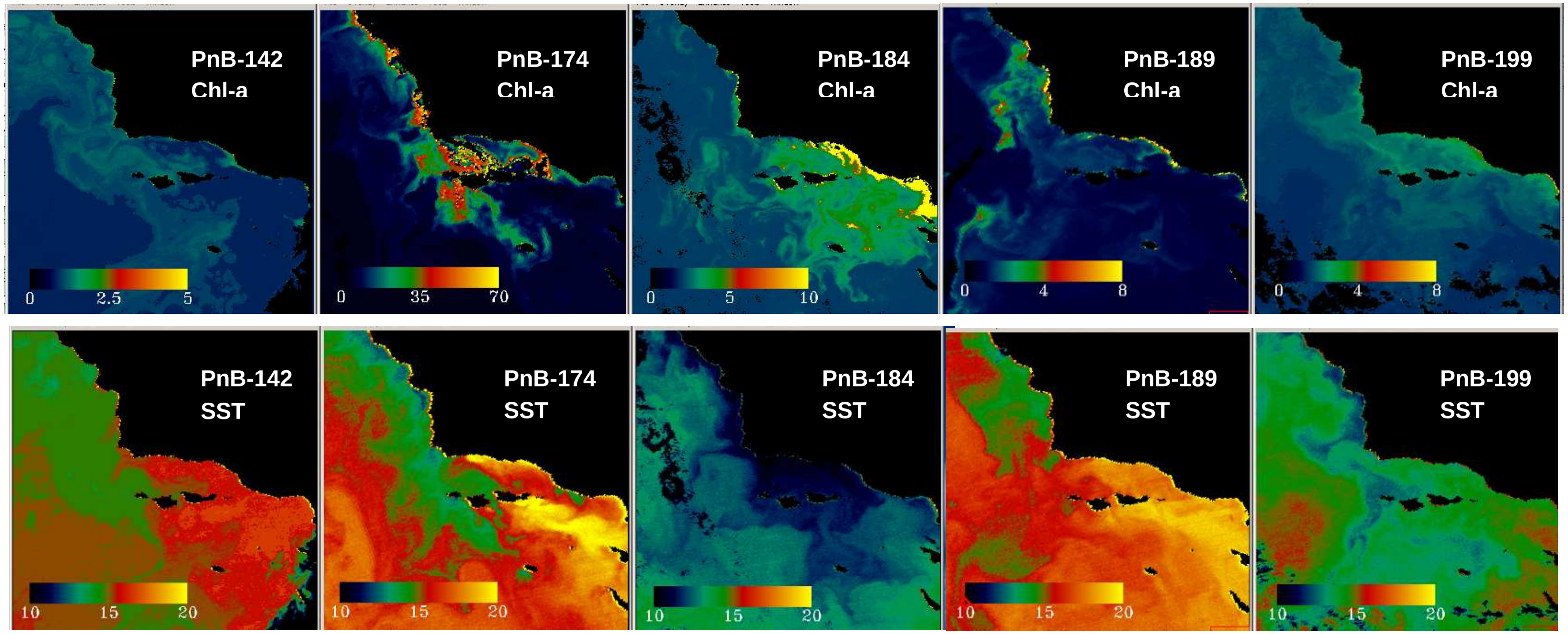

PnB-142: winter
PnB-174: spring/summer
PnB-184: spring
PnB-189: fall/winter
PnB-199: winter

MODIS L2 chlorophyll-a (chl-a) , in mg/m^3 and sea surface temperature (SST) in ^0C for the Southern California region. The Channel Islands can be seen masked in black in the centre of the images.

Observe the variability of chlorophyll-*a* and SST throughout the seasons. In between two seasons (PnB-174 and PnB-189), special productivity conditions are apparently enhanced, probably due to changes in the atmospheric conditions. Winter images may present warmer waters due to mixture of the water column after stronger winds. Also, observe the agreement between higher concentrations in chl-a and colder temperatures. The colour ramp scales were not accurately generated in this figure, but they rather give an idea of the concentrations at the time.

Appendix V

(Legend on next page)

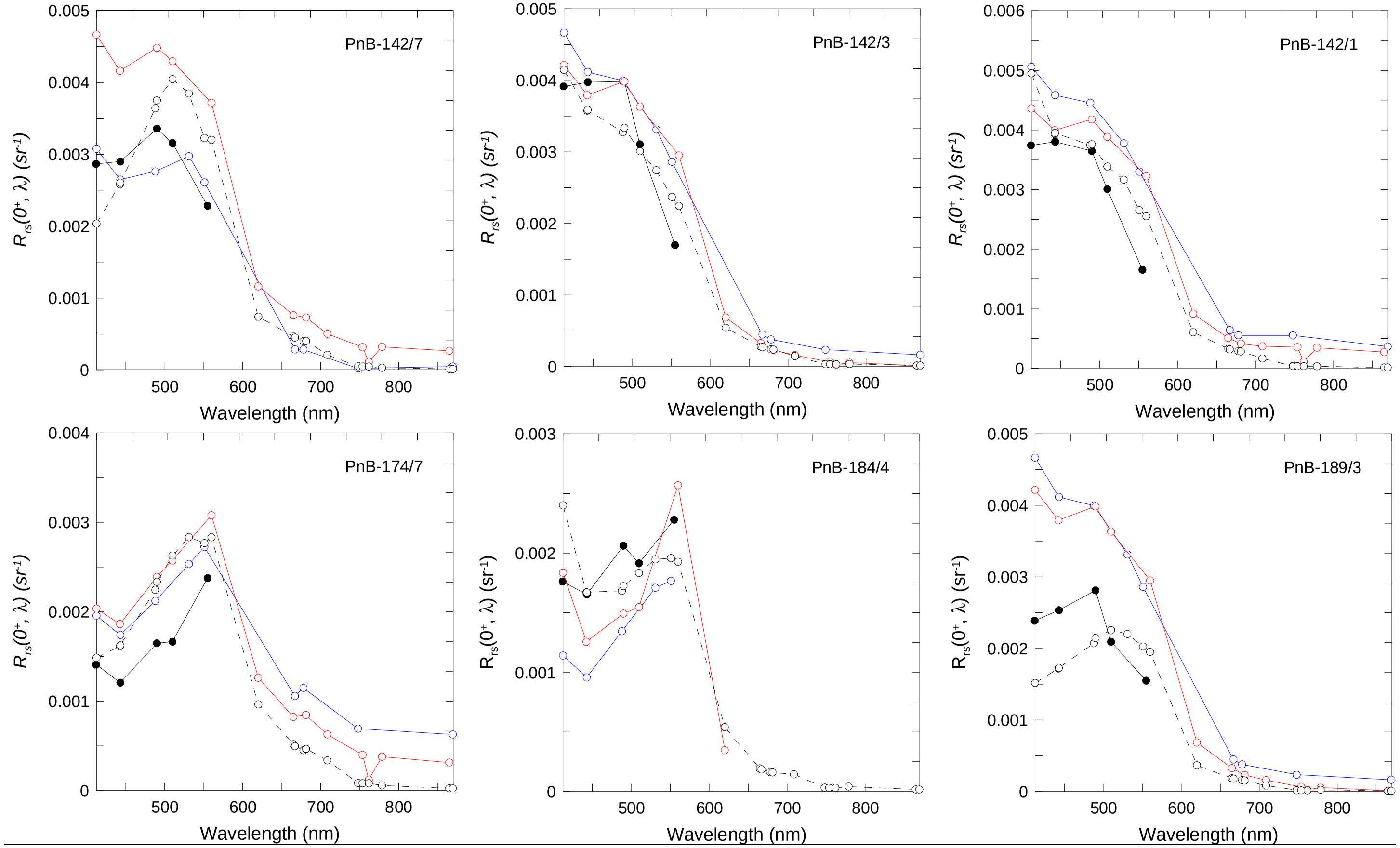

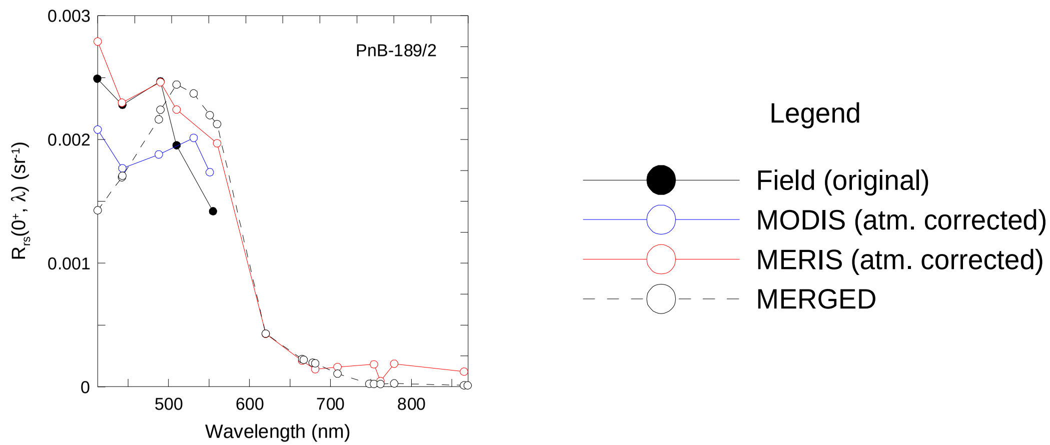

Figures in Appendix V compare the merged spectra (after applying the bio-optical modeling and the regression coefficients for 7 validations points) with the original field data, and the atmospherically corrected MODIS and MERIS data. On the right upper corner, cruise ID and station number. It is also possible to see how in some cases the merged spectra better approximates in shape to the measured field R_{rs}. In other cases, the maximum peaks are shifted, and further work will be necessary to investigate if that is a better approximation of what is happening in the environment, or if that is an artifact of the methodology.